Blended Response Algorithms for Linear Fluctuation-Dissipation for Complex Nonlinear Dynamical Systems

Rafail V. Abramov[1], **Andrew J. Majda**[2]

[1] Department of Mathematics, Statistics and Computer Science, University of Illinois at Chicago, 851 S. Morgan St., Chicago, IL 60607, USA

[2] Department of Mathematics and Center for Atmosphere Ocean Science, Courant Institute of Mathematical Sciences, New York University, 251 Mercer St., New York, NY 10012, USA

Abstract. In a recent paper the authors developed and tested two novel computational algorithms for predicting the mean linear response of a chaotic dynamical system to small changes in external forcing via the fluctuation-dissipation theorem (FDT): the short-time FDT (ST-FDT), and the hybrid Axiom A FDT (hA-FDT). Unlike the earlier work in developing fluctuation-dissipation theorem-type computational strategies for chaotic nonlinear systems with forcing and dissipation, these two new methods are based on the theory of Sinai-Ruelle-Bowen probability measures, which commonly describe the equilibrium state of such dynamical systems. These two algorithms take into account the fact that the dynamics of chaotic nonlinear forced-dissipative systems often reside on chaotic fractal attractors, where the classical quasi-Gaussian (qG-FDT) approximation of the fluctuation-dissipation theorem often fails to produce satisfactory response prediction, especially in dynamical regimes with weak and moderate degrees of chaos. It has been discovered that the ST-FDT algorithm is an extremely precise linear response approximation for short response times, but numerically unstable for longer response times. On the other hand, the hA-FDT method is numerically stable for all times, but is less accurate for short times. Here we develop blended linear response algorithms, by combining accurate prediction of the ST-FDT method at short response times with numerical stability of qG-FDT and hA-FDT methods at longer response times. The new blended linear response algorithms are tested on the nonlinear Lorenz 96 model with 40 degrees of freedom, chaotic behavior, forcing, dissipation, and mimicking large-scale features of real-world geophysical models in a wide range of dynamical regimes varying from weakly to strongly chaotic, and to fully turbulent. The results below for the blended response algorithms have a high level of accuracy for the linear response of both mean state and variance throughout all the different chaotic regimes of the 40-mode model. These results point the way toward the potential use of the blended response algorithms in operational long-term climate change projection.

AMS classification scheme numbers: 37N10,76F20,86A05,86A10

Submitted to: *Nonlinearity*

1. Introduction

The fluctuation-dissipation theorem (FDT) is one of the cornerstones of modern statistical physics, discovered about eighty years ago. Roughly speaking, the fluctuation-dissipation theorem states that for dynamical systems at statistical equilibrium the average response to small external perturbations can be calculated through the knowledge of suitable correlation functions of the unperturbed dynamical system. The fluctuation-dissipation theorem has great practical use in traditional settings involving statistical equilibrium of baths of identical gas or liquid molecules, Ornstein-Uhlenbeck Brownian motion, motion of electric charges, turbulence, quantum field theory, chemical physics, physical chemistry and other areas. The general advantage provided by the fluctuation-dissipation theorem is that one can successfully predict the response of a dynamical system at statistical equilibrium to an arbitrary small external perturbation without ever observing the behavior of the perturbed system, which offers great versatility and insight in understanding behavior of dynamical processes near equilibrium in numerous scientific applications [7, 13]. Typically, the linear response in the fluctuation-dissipation theorem is given as the time convolution of an external perturbation with the linear response operator in the form of a specially crafted time correlation function, which is computed through the long-term observation of the unperturbed dynamical system at statistical equilibrium. The latter fact explains the interest towards the fluctuation-dissipation theorem among the computational community, because one can often compute a long-time trajectory of a dynamical system near statistical equilibrium through a direct numerical simulation, and calculate the linear response "on the fly" as the numerical solution evolves by averaging its time series.

The fact that the fluctuation-dissipation theorem provides an approximation to the response of a dynamical system to a small change of its parameters by observing equilibrium statistical behavior of the unperturbed system makes it a convenient framework for studying long term global climate changes on the planetary scale. The response of climate dynamics on the planetary scale to changes of various global physical parameters is an area which is being extensively studied in contemporary atmosphere ocean science. The physical parameters controlling planetary climate dynamics range from solar radiation, to volcanic activity, greenhouse gases, ozone, polar ice melting and many others, which are normally computed via direct numerical simulation for an appropriate climate model. In the context of the fluctuation-dissipation theorem, one observes climatology of a model for a sufficiently long time under the tacit assumption that the dynamics is close to its statistical equilibrium, and then applies the fluctuation-dissipation theorem to predict mean climate response to small changes of the physical parameters of the dynamics without actually simulating an appropriate scenario of climate development for those changes of parameters, which usually poses a computational problem of substantial complexity.

Despite the fact that the climate system is a complex chaotic multiscale problem

with forcing, dissipation, and the equilibrium state structure has significant complexity, there has been a profound interest among the atmospheric/ocean science community to apply the fluctuation-dissipation theorem to predict global climate changes responding to variation of certain physical parameters. In the mid 1970s Leith [14] suggested the possibility that, despite the absence of the classical Gaussian equilibrium state, the fluctuation-dissipation theorem might constitute a sensible approximation for appropriate variables in the complex climate system. Leith's approximation has been called the quasi-Gaussian (qG-FDT) approximation in [17], where it is studied theoretically and computationally. Leith's suggestion has inspired others such as Bell [3], Carnevale et al. [4], and Dymnikov, Gritsoun and Branstator [8, 10, 12] to apply the quasi-Gaussian fluctuation-dissipation theorem for idealized climate models with various approximations and numerical procedures. Bell [3] considered a special truncation of the barotropic vorticity equation and studied the response of this truncation to small kick of trajectory at initial time, reporting that the predictions of classical FDT for the response of the system hold extremely well. Carnevale et al. [4] generalize the Gaussian FDT formula to a non-Gaussian, although smooth, equilibrium state, also documenting reasonably high precision of the classical Gaussian FDT formula for one model [18], but also its poor approximation for the classical Lorenz 63 model. Dymnikov, Gritsoun and Branstator [8, 10, 12] developed a systematic procedure to compute the complete linear response operator in the matrix form for different response times, and also present a robust algorithm of verification for the FDT response prediction through a series of direct numerical simulations with the actual perturbed system. Gritsoun and Branstator [9], and Gritsoun, Branstator and Majda [11] for computing the response of the mean state and variance, respectively, have applied the quasi-Gaussian approximation to a comprehensive general circulation model with interesting results. Craig and Cohen [5] applied the ideas of the classical FDT to the unresolved features of tropical convection and cloud formation.

The linear response of the forced-dissipative 40-mode Lorenz 96 model [1, 15, 16] within the framework of the quasi-Gaussian FDT has also been studied by the authors in [17]. It has been found in [17] that although the quasi-Gaussian FDT works reasonably well for the forced-dissipative Lorenz 96 model in strongly chaotic dynamical regimes, for weakly chaotic regimes the predictions of the classical FDT become much worse. While suitable for dynamical systems with a nearly canonical Gaussian equilibrium state, the fluctuation-dissipation theorem in its classical formulation is only partially successful for nonlinear dynamical systems with forcing and dissipation. The major difficulty in this situation is that the probability measure in the limit as time approaches infinity in this case is typically a Sinai-Ruelle-Bowen probability measure which is supported on a large-dimensional (often fractal) set and is usually not absolutely continuous with respect to the Lebesgue measure [6, 22]. In the context of Axiom A attractors, Ruelle [20, 21] has adapted the classical calculations for FDT to this setting.

In a recent paper [2], the authors develop and test two novel computational algorithms for predicting the mean linear response of a chaotic dynamical system to

small change in external forcing via the fluctuation-dissipation theorem (FDT): the short-time FDT (ST-FDT), and the hybrid Axiom A FDT (hA-FDT). Unlike the earlier work in developing fluctuation-dissipation theorem-type computational strategies for chaotic nonlinear systems with forcing and dissipation, the new FDT methods in [2] are based on the theory of Sinai-Ruelle-Bowen probability measures, which commonly describe the equilibrium state of such dynamical systems. The two algorithms take into account the fact that the dynamics of chaotic nonlinear forced-dissipative systems often reside on chaotic fractal attractors, where the classical quasi-Gaussian formula of the fluctuation-dissipation theorem often fails to produce satisfactory response prediction, especially in dynamical regimes with weak and moderate degrees of chaos. It has been discovered in [2] that the ST-FDT algorithm is an extremely precise linear response approximation for short response times, but numerically unstable for longer response times. On the other hand, the hA-FDT method is numerically stable for all times; however its derivation requires the dynamical system to satisfy Smale's Axiom A to constitute formally correct approximation, and at short times hA-FDT is not as precise as ST-FDT even for a simple nonlinear chaotic model with 5 degrees of freedom. Here we develop two blended algorithms which combine the precision of the ST-FDT method and numerical stability of either the classical qG-FDT or the hA-FDT approaches. The new algorithms are tested for the complex nonlinear Lorenz 96 model with 40 degrees of freedom [15–17] and large-scale features of real-world geophysical models in a wide range of dynamical regimes varying from weakly to strongly chaotic, and to fully turbulent. The results below demonstrate a sufficient level of precision for the blended response algorithms to be potentially useful in operational long-term climate change predictions for both linear and nonlinear response functions.

The current work is organized as follows. In Section 2 we introduce the ST-FDT and hA-FDT algorithms, as well as the classical quasi-Gaussian FDT formula (qG-FDT) from [17]. The ST-FDT and hA-FDT methods have opposing strengths and weaknesses: the ST-FDT method applies for a largely arbitrary dynamical system, and is a perfect approach to evaluate linear response of an arbitrary system for short times but suffers from numerical instability for longer times; the hA-FDT method is a rational approximation of Ruelle's FDT formula for an Axiom A attractor and is a better approximation for longer times in weakly and moderately chaotic dynamical regimes, where the quasi-Gaussian FDT approximation does not work well, as shown in [2]. Section 3 introduces the 40-mode nonlinear forced-dissipative Lorenz 96 (L96) model with remarkable mixing properties and an adjustable degree of chaos through a variable external forcing parameter. The Lorenz 96 model is developed by Lorenz and Emanuel in [15,16] as a relatively simple (by atmospheric/ocean science standards) nonlinear model with forcing and dissipation which mimics behavior of Rossby waves in complex geophysical models. In Section 4 we demonstrate the performance of the ST-FDT, hA-FDT and qG-FDT methods for the L96 model in a variety of weakly and strongly chaotic dynamical regimes. Section 5 features the new blended ST/hA-FDT and ST/qG-FDT algorithms which combine the precision of the ST-FDT method

and numerical stability of hA-FDT and qG-FDT algorithms. In Section 5 we also systematically test the new blended ST/hA-FDT and ST/qG-FDT algorithms for the L96 model in a variety of dynamical regimes and compare their performance to the ST-FDT, hA-FDT and qG-FDT methods for a simple linear response function. Section 6 contains the results of the testing of the blended ST/qG-FDT algorithm with a simple quadratic response function. In Section 7 we have concluding remarks on the results of the current work.

2. Approximate algorithms for linear response

Here we start with the fluctuation-dissipation theorem in its classical formulation for a dynamical system of chaotic ODEs for a vector $\vec{x} \in \mathbb{R}^N$, given by

$$\frac{\mathrm{d}\vec{x}}{\mathrm{d}t} = \vec{f}(\vec{x}), \tag{2.1}$$

where $\vec{f}$ is a vector field of dimension N. As discussed in [19], and also in Chapter 2 of [17], in the statistical dynamics of complex systems one is interested in the evolution of probability densities, $p(t, \vec{x})$, associated with (2.1) rather than individual solutions. It is well-known that the evolution of these probability densities, $p(t, \vec{x})$, satisfies the Liouville equation [19]

$$\begin{aligned} \frac{\partial}{\partial t} p(t, \vec{x}) &= L_L p(t, \vec{x}), \\ p(t, \vec{x})|_{t=0} &= p_0(\vec{x}), \end{aligned} \tag{2.2}$$

with $L_L p = -\operatorname{div}(\vec{f} p)$ being the Liouville operator.

The dynamical system in (2.1) is perturbed by small external forcing, $\delta\vec{f}(t, \vec{x})$, as

$$\frac{\mathrm{d}\vec{x}}{\mathrm{d}t} = \vec{f}(\vec{x}) + \delta\vec{f}(t, \vec{x}). \tag{2.3}$$

Then, similar to (2.2), the probability density $p^\delta(t, \vec{x})$ of the perturbed system in (2.3) satisfies an appropriately perturbed Liouville equation,

$$\begin{aligned} \frac{\partial}{\partial t} p^\delta(t, \vec{x}) &= L_L p^\delta(t, \vec{x}) + \delta L_L p^\delta(t, \vec{x}), \\ p^\delta(0, \vec{x}) &= p_0^\delta(\vec{x}), \end{aligned} \tag{2.4}$$

with $\delta L_L p = -\operatorname{div}(\delta\vec{f}(t, \vec{x}) p)$ being the part of the Liouville operator corresponding to small perturbation $\delta\vec{f}$ in (2.3). By $p_{eq}(\vec{x})$ we denote smooth rapidly decreasing (as $\|\vec{x}\| \to \infty$) equilibrium probability density for the unperturbed system in (2.2), so that

$$L_L p_{eq} = 0. \tag{2.5}$$

Further we assume a natural explicit time-space separable structure for the perturbation $\delta\vec{f}(t, \vec{x})$ in (2.3):

$$\delta\vec{f}(t, \vec{x}) = a(\vec{x})\delta\vec{f}(t), \tag{2.6}$$

with $a(\vec{x})$ being an $\vec{x}$-dependent matrix, and $\delta\vec{f}(t)$ being the time-dependent part of external forcing. Then, the Liouville operator δL_L in (2.4) can be written concisely as

$$\delta L_L p = \vec{L}_a p \cdot \delta\vec{f}(t) \tag{2.7}$$

with operator $\vec{L}_a$ given by

$$\vec{L}_a p = -\operatorname{div}(a(\vec{x})p). \tag{2.8}$$

In (2.8), the divergence of the matrix $a(\vec{x})p$ is a vector. In the case of space-independent external forcing $\delta\vec{f}(t,\vec{x}) = \delta\vec{f}(t)$ (so that $a(\vec{x})$ is the identity matrix) $\vec{L}_a$ assumes a simple form

$$\vec{L}_a p = -\nabla p. \tag{2.9}$$

Let $A(\vec{x})$ be a linear or nonlinear function whose mean response to small external forcing is to be predicted by the fluctuation-dissipation theorem. Here we assume that A is a scalar, however generalization to the vector-valued A is straightforward. The mean state, or expected value, of $A(\vec{x})$ with respect to the equilibrium probability density in (2.5) is, by definition, given by

$$E[A(\vec{x})] = \int_{\mathbb{R}^N} A(\vec{x}) p_{eq}(\vec{x}) \mathrm{d}\vec{x}. \tag{2.10}$$

The main statement of the fluctuation-dissipation theorem provides a formal procedure to calculate the change in expected value $\delta E[A(\vec{x})](t)$ for the perturbed system in (2.4) as

$$\delta E[A(\vec{x})](t) = \int_{\mathbb{R}^N} A(\vec{x}) \delta p(t,\vec{x}) \mathrm{d}\vec{x} = \int_0^t \vec{R}(t-t') \cdot \delta\vec{f}(t') \mathrm{d}t', \tag{2.11}$$

where the vector linear response operator is given by

$$\vec{R}(t) = \int_{\mathbb{R}^N} A(\vec{x}) \left(\exp[tL_L][\vec{L}_a p_{eq}] \right)(\vec{x}) \mathrm{d}\vec{x}. \tag{2.12}$$

Note that the formula (2.12) depends only on the equilibrium state density p_{eq}, which means that behavior of the perturbed system from (2.4) does not need to be observed to compute (2.12). Formal systematic derivation of (2.11) and (2.12) is given in [19], and also Chapter 2 of [17]). For the special case with constant external forcing $\delta\vec{f} = const$ the linear response formula is simplified to

$$\delta E[A(\vec{x})](t) = \vec{\mathcal{R}}(t) \cdot \delta\vec{f}, \qquad \vec{\mathcal{R}}(t) = \int_0^t \vec{R}(t') \mathrm{d}t', \tag{2.13}$$

where $\vec{R}(t)$ is taken from (2.12). The general formula in (2.12) serves as the starting point for further approximations under various assumptions, leading to different versions of the fluctuation-dissipation theorem.

2.1. Short-time FDT (ST-FDT)

A wide variety of practical geophysical models are complex nonlinear chaotic forced-dissipative dynamical systems, whose solutions live on strange attractors. The equilibrium states on such attractors do not even possess densities p_{eq} with respect to Lebesgue measure. Here and below we assume that the dynamical system is ergodic and mixing [22] with decay of time correlation functions so that averages over the equilibrium measure can be replaced by a long time average [2, 17]. The authors in [2] rework the classical FDT formula in (2.12) and (2.13) in such a way that an approximation to the density p_{eq} of the equilibrium probability measure is not required to compute the linear response. This method is called short-time FDT (ST-FDT), due to its inherent numerical instability at longer times for chaotic dynamical systems, and is given by the formula

$$\vec{R}_{ST-FDT}(\tau) = \lim_{r\to\infty} \frac{1}{r} \int_0^r \nabla A\left(\vec{x}(t+\tau)\right) T^{\tau}_{\vec{x}(t)} a(\vec{x}(t)) \mathrm{d}t, \tag{2.14}$$

where $T^{\tau}_{\vec{x}}$ is a tangent map at $\vec{x}$ to τ

$$T^{\tau}_{\vec{x}(t)} = \exp\left(\int_t^{t+\tau} \nabla \vec{f}(\vec{x}(s)) \mathrm{d}s\right), \tag{2.15}$$

which can be obtained by solving the equation

$$\frac{\mathrm{d}T^{\tau}_{\vec{x}(t)}}{\mathrm{d}\tau} = \nabla \vec{f}(\vec{x}(t+\tau)) T^{\tau}_{\vec{x}(t)}. \tag{2.16}$$

For constant external forcing δf, the formula (2.13) is written here as

$$\begin{aligned} \delta E[A(\vec{x})]_{ST-FDT}(t) &= \vec{\mathcal{R}}_{ST-FDT}(t) \cdot \delta \vec{f}, \\ \vec{\mathcal{R}}_{ST-FDT}(s) &= \lim_{r\to\infty} \frac{1}{r} \int_0^r \mathrm{d}t \int_0^s \nabla A\left(\vec{x}(t+\tau)\right) T^{\tau}_{\vec{x}(t)} \mathrm{d}\tau. \end{aligned} \tag{2.17}$$

Note that the linear response formulas in (2.14) and (2.17) do not include the equilibrium probability density p_{eq}. The latter property makes them suitable for computing the linear response for an arbitrary equilibrium state, even if it does not possess probability density with respect to the Lebesgue measure. The main drawback of (2.14) and (2.17) is that the tangent map in (2.15) undergoes exponential blow-up in time due to the presence of positive Lyapunov characteristic exponents in chaotic dynamical systems, and thus (2.14) and (2.17) can only be used for limited time intervals.

2.2. Classical quasi-Gaussian FDT (qG-FDT)

Following the derivation in [19] or Chapter 2 of [17], the classical FDT formula for the linear response vector $\vec{R}(t)$ in (2.12) is expressed as the time autocorrelation function

$$\vec{R}(\tau) = \langle A(\vec{x}(t+\tau)) \vec{B}(\vec{x}(t)) \rangle, \tag{2.18}$$

where the long-term trajectory $\vec{x}(t)$ is observed for the unperturbed system, with the special function $\vec{B}(\vec{x})$,

$$\vec{B}(\vec{x}) = \frac{\vec{L}_a(\vec{x}) p_{eq}(\vec{x})}{p_{eq}(\vec{x})}, \tag{2.19}$$

where the correlation vector on the right hand size of (2.18) is evaluated at the unperturbed state. The quasi-Gaussian FDT (qG-FDT) approximation is obtained from (2.18) and (2.19) by replacing the equilibrium probability density p_{eq} with its Gaussian approximation p_G

$$p_G(\vec{x}) = \frac{1}{(2\pi \det \sigma^2)^{N/2}} \exp\left(-\frac{1}{2}(\vec{x}-\bar{\vec{x}})\sigma^{-2}(\vec{x}-\bar{\vec{x}})\right), \tag{2.20}$$

with the mean state $\bar{\vec{x}}$ and covariance matrix σ^2 matching those of p_{eq}. Additionally, here it is assumed that the external forcing $\delta\vec{f}$ is $\vec{x}$-independent such that $\vec{L}_a$ has the simplified form in (2.9). Under these assumptions, the function $B(\vec{x})$ from (2.19) becomes

$$B_G(\vec{x}) = \sigma^{-2}(\vec{x}-\bar{\vec{x}}), \tag{2.21}$$

and the formula for the kernel $\vec{R}(\tau)$ of the linear response operator becomes a simple time autocorrelation function

$$\vec{R}_{qG-FDT}(\tau) = \lim_{r\to\infty}\frac{1}{r}\int_0^r A(\vec{x}(t+\tau))\sigma^{-2}(\vec{x}(t)-\bar{\vec{x}})\mathrm{d}t. \tag{2.22}$$

For constant external forcing $\delta\vec{f}$, the formula (2.13) is written here as

$$\begin{aligned} \delta E[A(\vec{x})]_{qG-FDT}(t) &= \vec{\mathcal{R}}_{qG-FDT}(t)\cdot\delta\vec{f}, \\ \vec{\mathcal{R}}_{qG-FDT}(s) &= \lim_{r\to\infty}\frac{1}{r}\int_0^r \mathrm{d}t\int_0^s A(\vec{x}(t+\tau))\sigma^{-2}(\vec{x}(t)-\bar{\vec{x}})\mathrm{d}\tau. \end{aligned} \tag{2.23}$$

The prefix "quasi" in the name of the quasi-Gaussian FDT formula comes from the fact that although the equilibrium density p_{eq} in the linear response operator is simplified by the Gaussian approximation, the time averaging process in (2.22) corresponds to the phase space averaging with respect to the true equilibrium state, rather than its Gaussian approximation. For details, see Chapter 2 of [17]. This is the form of FDT advocated by Leith [14] in his seminal paper. Section 2.7 of [17] contains a rigorous analysis of the validity of this approximation for short times.

2.3. Hybrid Axiom A FDT (hA-FDT)

The main drawback of the ST-FDT formula in (2.14) is that it can only be used for limited time intervals of τ, due to the fact that the tangent map $T^\tau_{\vec{x}}$ undergoes exponential blow-up in the directions associated with positive Lyapunov characteristic exponents. Here, under the assumption of an Axiom A flow $\vec{X}(t,\vec{x})$ which settles onto a strange attractor $\mathcal{K}$, we avoid numerical instability in the short-time FDT approach in (2.14) by following the directions given in [21].

With help of Axiom A, one can uniformly decompose the small perturbation $\delta\vec{f}(t,\vec{x})$ into the sum of three components at each point of the trajectory $x(t)$ on the attractor:

$$\delta\vec{f}(t,\vec{x}) = P^+_{\vec{x}}\delta\vec{f}(t,\vec{x}) + P^-_{\vec{x}}\delta\vec{f}(t,\vec{x}) + P^0_{\vec{x}}\delta\vec{f}(t,\vec{x}), \tag{2.24}$$

where $P^+_{\vec{x}}$, $P^-_{\vec{x}}$ and $P^0_{\vec{x}}$ are the projection operators onto the expanding subspace $E^+_{\vec{x}}$, contracting subspace $E^-_{\vec{x}}$ and neutrally stable subspace E^0, consisting of only one vector $\vec{f}(\vec{x})$ (which is tangent to the direction of trajectory $\vec{x}(t)$), of the tangent bundle $T\mathcal{K}$

over the strange attractor $\boldsymbol{\kappa}$ at $\vec{x}$. From a practical standpoint, $P^+_{\vec{x}}$ projects onto the span of the eigenvectors for positive Lyapunov exponents at $\vec{x}$, and $P^-_{\vec{x}}$ projects onto the span of the eigenvectors for negative Lyapunov exponents at $\vec{x}$. The neutral direction corresponds to zero Lyapunov exponent. For rigorous definition and detailed description of $E^+_{\vec{x}}$ and $E^-_{\vec{x}}$ see [6]. All projection operators in (2.24) are computed from the tangent map $T^\tau_{\vec{x}}$ (see [2] for numerical algorithm).

With (2.24), (2.14) becomes

$$\vec{R}_{A-FDT}(\tau) = \vec{R}^+(\tau) + \vec{R}^{0-}(\tau), \tag{2.25}$$

with the corresponding expanding and neutral-contracting response operators

$$\vec{R}^+(\tau) = \lim_{r\to\infty} \frac{1}{r} \int_0^r \nabla A(\vec{x}(t+\tau)) T^\tau_{\vec{x}(t)} P^+_{\vec{x}(t)} a(\vec{x}(t)) \mathrm{d}t, \tag{2.26a}$$

$$\vec{R}^{0-}(\tau) = \lim_{r\to\infty} \frac{1}{r} \int_0^r \nabla A(\vec{x}(t+\tau)) T^\tau_{\vec{x}(t)} (P^0_{\vec{x}(t)} + P^-_{\vec{x}(t)}) a(\vec{x}(t)) \mathrm{d}t. \tag{2.26b}$$

A rational approximation to the expanding response operator, $\vec{R}^+(\tau)$ in the Axiom A FDT formula in (2.26a) is developed by the authors in [2]. One reason for this is the numerical difficulty noted above in reliably calculating the unstable divergence. A second, more fundamental reason is that it is doubtful that most realistic physical systems have Axiom A attractors anyway, so an exact solution formula for A-FDT would still involve an approximation, and, therefore, a different rational approximation might be appropriate. For the hA-FDT approximation, we replace the ST-FDT approximation projected onto the uniformly expanding directions in (2.26a) with the qG-FDT approximation, using the fact that an SRB measure is smooth along the uniformly expanding directions [6, 22]. The result is the hybrid A-FDT (hA-FDT) approximation

$$\vec{R}^+_{hA-FDT}(\tau) = \lim_{r\to\infty} \frac{1}{r} \int_0^r A(\vec{x}(t+\tau)) P^+_{\vec{x}(t)} \sigma^{-2} (\vec{x}(t) - \bar{\vec{x}}) \mathrm{d}t. \tag{2.27}$$

If this formula is combined with the formula in (2.26b) for $\vec{R}^{0-}(\tau)$ involving the response for the contracting directions, for constant external forcing we obtain the hybrid A-FDT approximation:

$$\delta E[A(\vec{x})]_{hA-FDT}(t) = \vec{\mathcal{R}}_{hA-FDT}(t) \cdot \delta \vec{f}, \tag{2.28a}$$

$$\vec{\mathcal{R}}_{hA-FDT}(t) = \vec{\mathcal{R}}^+_{hA-FDT}(t) + \vec{\mathcal{R}}^{0-}_{hA-FDT}(t), \tag{2.28b}$$

$$\vec{\mathcal{R}}^+_{hA-FDT}(s) = \lim_{r\to\infty} \frac{1}{r} \int_0^r \mathrm{d}t \int_0^s A(\vec{x}(t+\tau)) P^+_{\vec{x}(t)} \sigma^{-2} (\vec{x}(t) - \bar{\vec{x}}) \mathrm{d}\tau, \tag{2.28c}$$

$$\vec{\mathcal{R}}^{0-}_{hA-FDT}(s) = \lim_{r\to\infty} \frac{1}{r} \int_0^r \mathrm{d}t \int_0^s \nabla A(\vec{x}(t+\tau)) T^\tau_{\vec{x}(t)} (P^0_{\vec{x}(t)} + P^-_{\vec{x}(t)}) \mathrm{d}\tau. \tag{2.28d}$$

2.4. Validation of linear response approximations

In order to assess advantages and drawbacks of various linear response approximations, one has to verify correctness of the results they provide. We validate the performance of the linear response approximations against the so-called "ideal response" operator, $\vec{\mathcal{R}}_I$, which is the actual directly measured response of the model, perturbed by series of small external forcing perturbations. To compute the ideal response, these small perturbations are applied to a large statistical ensemble of solutions ($\sim$ 100000 members) to ensure sufficient precision in measuring the mean linear response. This algorithm for the ideal response operator has been developed by Gritsoun and Dymnikov [12], and has been used for validation of classical FDT response for various chaotic dynamical systems in [17].

3. The L96 model: A testbed for linear response in complex dynamical systems

The 40-mode Lorenz 96 model (L96) has been introduced by Lorenz and Emanuel [15,16] as a simple model with large scale features of complex nonlinear geophysical systems. The L96 model is given by

$$\frac{\mathrm{d}x_j}{\mathrm{d}t} = (x_{j+1} - x_{j-2})x_{j-1} - x_j + F, \quad j = 1 \dots 40 \tag{3.1}$$

with periodic boundary conditions. As mentioned before, the L96 model possesses some general properties of geophysical models, namely energy-preserving nonlinear term mimicking advection, linear damping $-x_j$ and constant forcing F. The model in (3.1) is designed to mimic midlatitude weather and climate behavior, so periodic boundary conditions are appropriate. The unit spatial scale between discrete nodes is regarded as a non-dimensional midlatitude Rossby radius $\approx$ 800 km; the discrete system with 40 modes corresponds to a midlatitude belt of roughly 30000 km. In midlatitude weather systems, the main "weather waves", the Rossby waves, have westward (toward negative x) phase velocity, but eastward group velocity. For the values of constant forcing F ranging from 5 to 32 the Lorenz 96 model has the band of linearly unstable wave, located roughly between the Fourier wavenumbers 3 and 12 (which slightly varies with different values of F). It is shown in [15, 16] and Chapter 2 of [17] that this band of linearly unstable wavenumbers has westward phase and eastward group velocities, just like actual Rossby waves. The complete list of parameters and numerical techniques for these models follows below.

It is demonstrated in Chapter 2 of [17] that the dynamical regime of the L96 model varies with changing the value of constant forcing F: weakly chaotic dynamical regimes with $F = 5, 6$, strongly chaotic regime with $F = 8$, and turbulent regimes $F = 12, 16, 24$ with self-similar time autocorrelation decay. In this section we demonstrate the following dynamical properties of the L96 model:

- λ_1 – the value of the largest Lyapunov exponent, which indicates the rate with which two nearby trajectories $\vec{x}(t)$ diverge from each other,

- N^+ – the dimension of the uniformly expanding subspace of the tangent bundle over the chaotic attractor, which is also the number of positive Lyapunov exponents,
- KS – the Kolmogorov-Sinai entropy, which is a sum of all positive Lyapunov exponents, constituting a basic measure of chaos in the system,
- $\mathcal{T}_c$ – the autocorrelation function decay time, which is computed as a time integral of the absolute value of the time autocorrelation function for $x_j(t)$ in (3.1)

$$C(\tau) = \langle (x_j(t) - \bar{x})(x_j(t+\tau) - \bar{x}) \rangle_t, \quad \mathcal{T}_c = \int_0^\infty |C(\tau)| \mathrm{d}\tau. \tag{3.2}$$

  In practice, the integral is computed for sufficiently large (but not infinite) values of τ. $\mathcal{T}_c$ is rescaled by the mean energy of perturbations of the L96 model like in Chapter 2 of [17] to reveal self-similarity of time autocorrelation functions for the turbulent regimes $F = 12, 16, 24$. Small values of $\mathcal{T}_c$ indicate mixing dynamical regime and rapidly decaying time autocorrelation functions, whereas large values of $\mathcal{T}_c$ typically signify quasi-periodic weakly mixing dynamical regime.

We compute the above dynamical properties through direct numerical simulations with the L96 model and the following numerical parameters:

- Number of degrees of freedom $N = 40$;
- 4th-order Runge-Kutta time integrator;
- Numerical time step $\Delta t = 1/64$;
- Values of constant forcing $F = 5, 6, 8, 12, 16, 24$;
- Averaging time window for computing long-term time averages is $T = 500000$ time units;
- Initial spin-up time $T_0 = 10000$ is skipped before computing averages to let the numerical trajectory land on the attractor.

For details on computing the Lyapunov characteristic exponents and correlation times, see [2] and the Chapter 2 of [17].

Here in Table 1 we show the dynamical properties of the L96 model in the dynamical regimes $F = 5, 6, 8, 12, 16, 24$. Observe that the largest Lyapunov exponent λ_1, the dimension of uniformly expanding subspace N^+ and Kolmogorov-Sinai entropy KS systematically grow with increasing F, which indicates the increasing strength of chaos for dynamical regimes with larger F. On the other hand, the energy-rescaled correlation time $\mathcal{T}_c$ tends to decay while F increases from $F = 5$ to $F = 12$, but stays roughly same for the regimes $F = 12, 16$ and 24, which indicates strongly turbulent dynamical regimes with self-similar decay of time autocorrelation functions.

3.1. Ideal response of the L96 model for long times

It has been demonstrated in Chapter 2 of [17] that the relatively simple classical qG-FDT approximation can be remarkably precise for strongly chaotic turbulent regimes with large values of F, where L96 model in energy-rescaled variables approaches its

unforced undamped energy conserving counterpart with canonical Gaussian equilibrium probability state. On the other hand, observe that for for the simple response function $A(\vec{x}) = \vec{x}$, the qG-FDT approximation in (2.23) is essentially the time integral of the simple time autocorrelation function in (3.2). These two facts suggest that for strongly chaotic turbulent regimes $F = 12, 16, 24$, the time when the response of the L96 model to constant external forcing "saturates" and becomes constant should be of the same order as the autocorrelation time $\mathcal{T}_c$. The latter means that the ideal response for times much longer than the autocorrelation time is essentially the ideal response at infinite time. Also, self-similarity of the time autocorrelation functions for the regimes $F = 12, 16, 24$ suggests self-similarity of the ideal response of the L96 model for the same regimes.

Here we show the results of comparison for the ideal responses for the response function $A(\vec{x}) = \vec{x}$ at energy-rescaled times $T = 40$ and $T = 80$, which far exceed the autocorrelation times in Table 1. We quantify are two distinct aspects of error.

- The first aspect, which is the most obvious, is a bulk error between responses computed at different coordinates x_j for a given forcing, which can be quantified by a simple error norm, for example, Euclidean L_2-norm. The relative L_2-error between two response operators $\vec{\mathcal{R}}_1$ and $\vec{\mathcal{R}}_2$ is defined as

$$L_2\text{-error} = \frac{\|\vec{\mathcal{R}}_1 - \vec{\mathcal{R}}_2\|}{\|\vec{\mathcal{R}}_1\|}, \tag{3.3}$$

  where $\|\cdot\|$ denotes the norm generated by the standard Euclidean inner product.

- The second, less obvious aspect, is the similarity, or physical correlation between two response operators, which signifies the error in location of a response, rather than its strength. In a number of practical geophysical applications, predicting the correct location of some phenomena is often more important than predicting their magnitude at the same location [10]. In order to address the physical correlation, or similarity, between the two responses, we introduce a special physical space correlation function, which is defined as

$$Corr = \frac{(\vec{\mathcal{R}}_1, \vec{\mathcal{R}}_2)}{\|\vec{\mathcal{R}}_1\|\|\vec{\mathcal{R}}_2\|}, \tag{3.4}$$

  where $(\cdot, \cdot)$ is the standard Euclidean inner product. Thus, the L_2-error as defined in (3.3) indicates the bulk discrepancy between the FDT and ideal operators, whereas the $Corr$ function as defined in (3.4) signifies the collinearity of the two operators. The value of 1 of the $Corr$ function indicates complete collinearity between the two operators (without the regard of their magnitudes, which could be very different), and the value of 0 indicates complete decorrelation. Negative values of the physical correlation function provide the evidence that the two responses are anti-correlated.

In Table 1 we show the L_2-errors and physical space correlation functions between the ideal response operators at times $T = 40$ and $T = 80$. These times are chosen so that they exceed the autocorrelation times for turbulent self-similar dynamical regimes $F = 12, 16, 24$ roughly by an order of magnitude. Observe that the L_2-errors are small

for the regimes $F = 8, 12, 16, 24$, which essentially means that time $T = 80$ for these regimes can be considered equivalent to infinite time. On the other hand, the L_2-errors are not small for the weakly chaotic regimes $F = 5, 6$, which is expected, since the decay of correlation functions does not necessarily indicate the saturation of the ideal response, due to poor connection between the qG-FDT and ideal response for these regimes [17]. The physical space correlation functions confirm the same trend, with ideal responses for turbulent regimes being better correlated than those for weakly chaotic regimes.

In Table 2 and Figures 1 and 2 we show the physical space correlation and self-similarity of the ideal response in the regimes $F = 5, 6, 8, 12, 16$ directly compared with the most turbulent regime $F = 24$. Observe that the turbulent regimes $F = 12, 16$ correlate with the regime $F = 24$ remarkably well, also being visually very similar for both times $T = 40$ and $T = 80$, which confirms observations in [17] for turbulent self-similar regimes and good connection between simple time autocorrelation functions and the response of the L96 system to small constant external forcing for these regimes. On the other hand, the weakly chaotic regimes $F = 5, 6$ exhibit poor physical space correlations and visual similarity, which is also expected. The strongly chaotic regime $F = 8$, which is not yet fully turbulent, is better correlated with $F = 24$ than regimes with $F = 5, 6$, but not as good as the regimes with $F = 12, 16$.

4. Performance of the FDT algorithms on the testbed

Here we study the linear response of the three FDT methods, qG-FDT, ST-FDT and hA-FDT, and validate their performance against the ideal response operator, R_{ideal}, which is the actual directly measured response of the model, perturbed by series of small external forcing perturbations. To compute the ideal response, these small perturbations are applied to a large statistical ensemble of solutions ($\sim$ 100000 members) to ensure

40-mode L96 model						
F	λ_1	N^+	KS	$\mathcal{T}_C$	$L_2(40, 80)$	$Corr(40, 80)$
5	0.4726	9	1.811	14	0.2859	0.9584
6	1.02	12	5.547	8.23	0.2528	0.9675
8	1.74	13	10.94	6.704	0.1812	0.9834
12	2.937	15	20.12	5.9	0.1475	0.991
16	3.945	16	27.94	5.594	0.1683	0.9879
24	5.683	17	41.82	5.312	0.173	0.9851

Table 1. Dynamical properties of the L96 model in the regimes $F = 5, 6, 8, 12, 16, 24$. λ_1 – largest Lyapunov exponent, N^+ – dimension of the expanding subspace of the attractor, KS – Kolmogorov-Sinai entropy (sum of positive Lyapunov exponents), $\mathcal{T}_c$ – correlation time of energy-rescaled time correlation function, $L_2(40, 80)$ – relative L_2-error between $\vec{\mathcal{R}}_I(40)$ and $\vec{\mathcal{R}}_I(80)$, $Corr(40, 80)$ – physical space correlation function between $\vec{\mathcal{R}}_I(40)$ and $\vec{\mathcal{R}}_I(80)$.

40-mode L96 model, physical space correlations of the ideal response for different values of F					
	5 vs 24	6 vs 24	8 vs 24	12 vs 24	16 vs 24
$T = 40$	0.5927	0.8111	0.8937	0.9581	0.9811
$T = 80$	0.5403	0.7721	0.8897	0.9449	0.9761

Table 2. Physical space correlations of ideal responses between the most turbulent regime $F = 24$ and the regimes $F = 5, 6, 8, 12, 16$. Time $T = 40$ and $T = 80$.

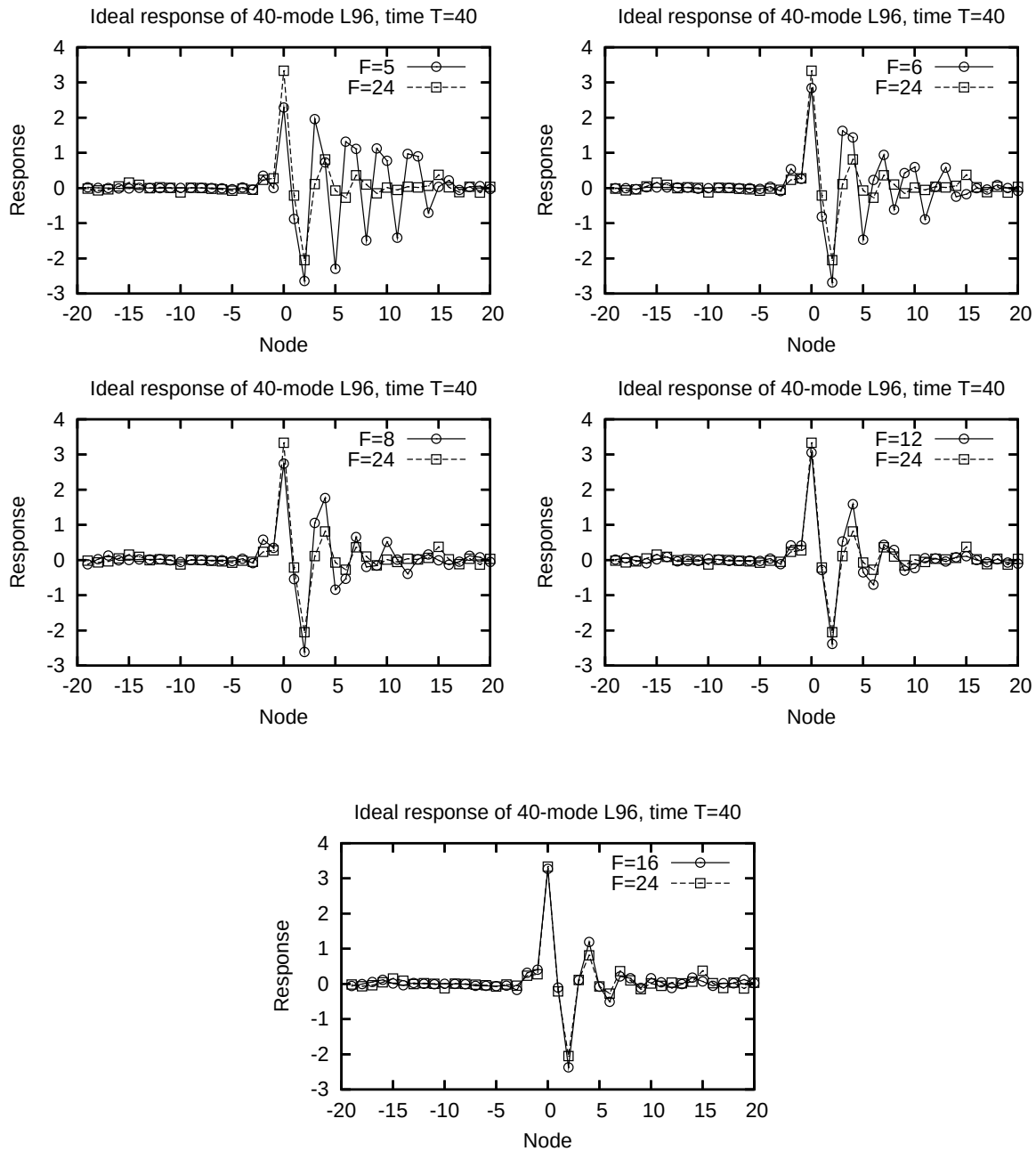

Figure 1. The self-similarity of ideal response profiles at $T = 40$.

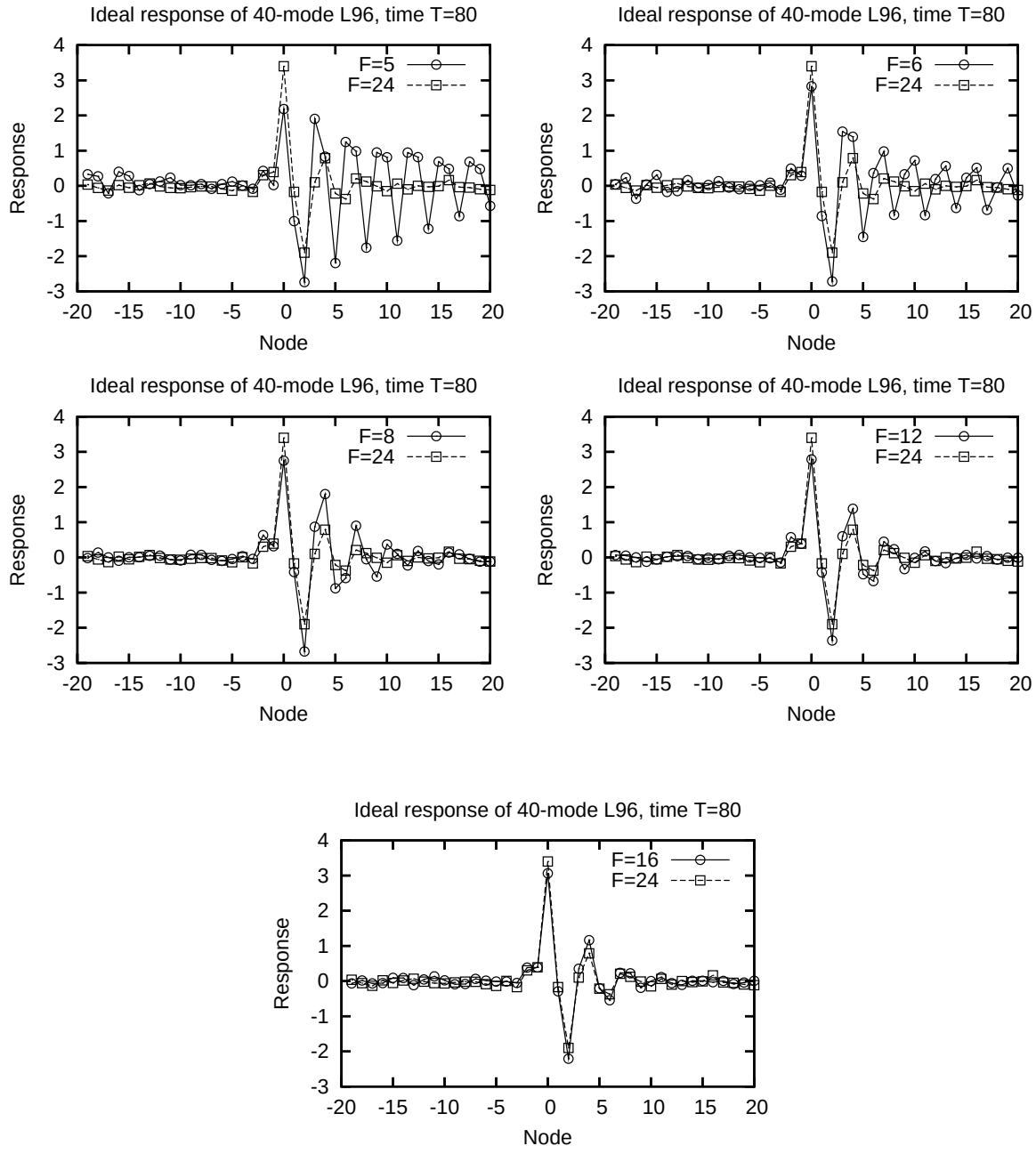

Figure 2. The self-similarity of ideal response profiles at $T = 80$.

sufficient precision in measuring the mean linear response. This ideal response operator has been developed by Gritsoun and Dymnikov [12], and has been used for validation of classical FDT response for various chaotic dynamical systems in [17]. For extensive description and numerical algorithms for the ideal response operator, see [12, 17]. The numerical parameters for FDT simulations for the L96 model essentially follow those used in Section 3:

- Number of degrees of freedom $N = 40$;
- 4th-order Runge-Kutta time integrator;
- Numerical time step $\Delta t = 1/64$;
- Values of constant forcing $F = 5, 6, 8, 12, 16, 24$;
- A simple linear vector-valued response function $\vec{A}(\vec{x}) = \vec{x}$;
- Averaging time window for computing long-term time averages is $T = 500000$ time units;
- Initial spin-up time $T_0 = 10000$ is skipped before computing averages to let the numerical trajectory land on the attractor;
- The response is measured for constant small external forcing.

As stated above, all response operators are computed for constant small external perturbations, and therefore we display the ST-FDT, qG-FDT and hA-FDT linear response operators from formulas (2.17), (2.23) and (2.28), respectively, rather than their convolution kernels in more general formulas for arbitrary time- and space-dependent external perturbations. Also observe that while the theory in Section 2 is developed for a scalar response function $A(\vec{x})$, the tested response functions above are vector-valued. As a result, the linear response operator $\mathcal{R}(\tau)$ becomes a matrix, rather than being vector in Section (2), which is a simple and straightforward generalization of scalar linear response function onto vector-valued response. However, since the 40-mode L96 model is translationally invariant (given its periodic boundary conditions), the columns of all linear response operators translate into each other along the main diagonal. Thus, rather than displaying linear response operators as matrices with translationally invariant columns, we show their middle (i.e. 20th for $N = 40$) columns, which correspond for response to unit external forcing at the middle coordinate. This is done to aid visualization and simplify comparative analysis of performance for different response operators. Additionally, validation of ideal response operators is done at the end of Section 4. The time scale for linear response measurements is appropriately rescaled by the energy of perturbations like in Chapter 2 of [17], to ensure consistent response time scales for different dynamical regimes regardless of their mean energy.

In Figure 3 we show the singular values 1,3,5,7 of the linear response operator for the linear response function $A(\vec{x}) = \vec{x}$ in the weakly chaotic dynamical regime $F = 5$. Due to translational invariance, singular values 2,4,6,8 are identical to the singular values 1,3,5,7, respectively, and the associated singular vectors are Fourier modes [2]. Note that the singular values of the qG-FDT response operator systematically overshoot the

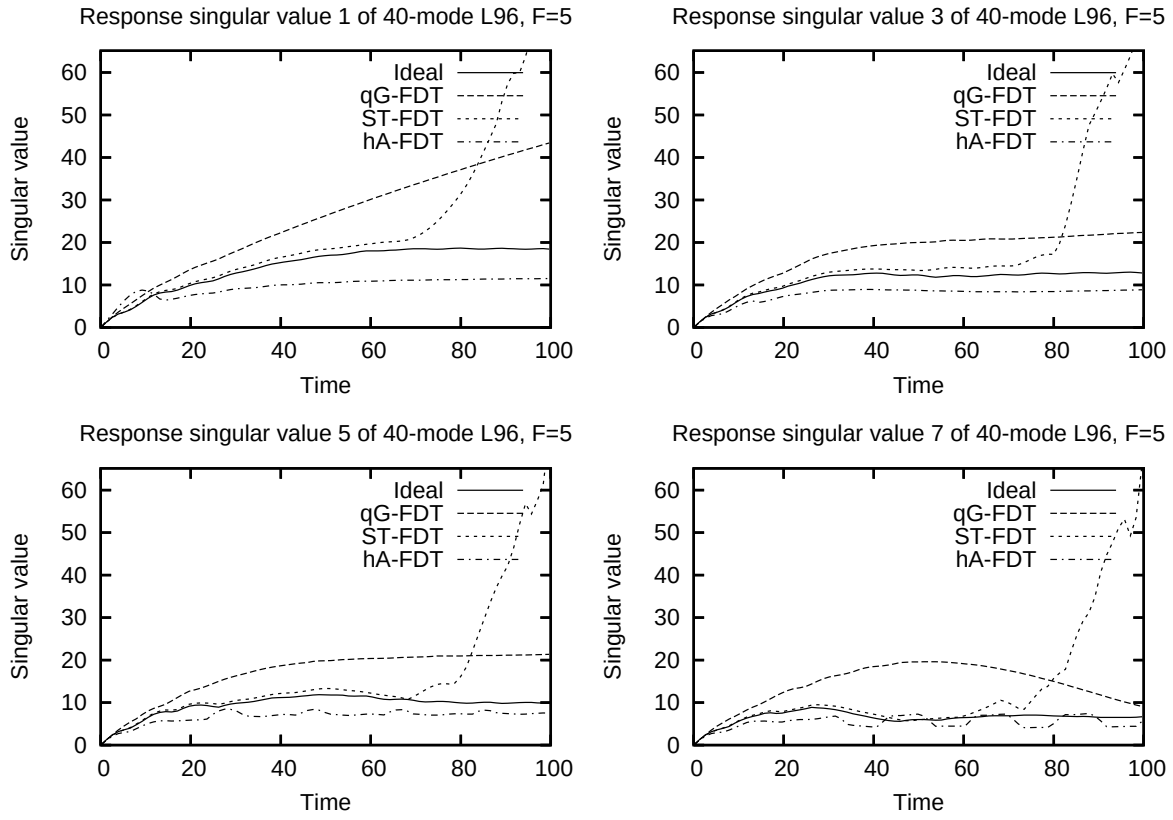

Figure 3. The singular values of the linear response operators for the regime $F = 5$, response function $A(\vec{x}) = \vec{x}$.

corresponding singular values of the ideal operator, while the hA-FDT singular values undershoot them. On the other hand, all displayed singular values of the ST-FDT operator closely follow the corresponding singular values of the ideal response operator, until a numerical instability manifests itself about time $T = 80$. As discussed before in Section 2, this numerical instability occurs due to the presence of positive Lyapunov exponents, which let the tangent map grow exponentially fast along uniformly expanding directions on the attractor.

In Figures 4 and 5 we demonstrate the snapshots of the linear response operators in the physical space (Figure 4) and Fourier space (Figure 5) in the weakly chaotic dynamical regime $F = 5$ at time $T = 40$ and $T = 80$. By sight, the hA-FDT response is more precise than the qG-FDT response for both times, $T = 40$ and $T = 80$, which is also confirmed in Tables 3 and 5 in Section 5 below, where the L_2-errors and physical space correlations for both the qG-FDT and hA-FDT response operators are shown. The ST-FDT response operator is very precise at $T = 40$ (much better than either qG-FDT or hA-FDT), however it is completely inaccurate at $T = 80$ due to numerical instability. Figure 5 explains why the hA-FDT operator is superior to qG-FDT; it turns out that the hA-FDT operator in Figure 5 is a reasonably good approximation for linearly stable Fourier modes with low wavenumbers $k < 3$, where the qG-FDT operator is the most erroneous.

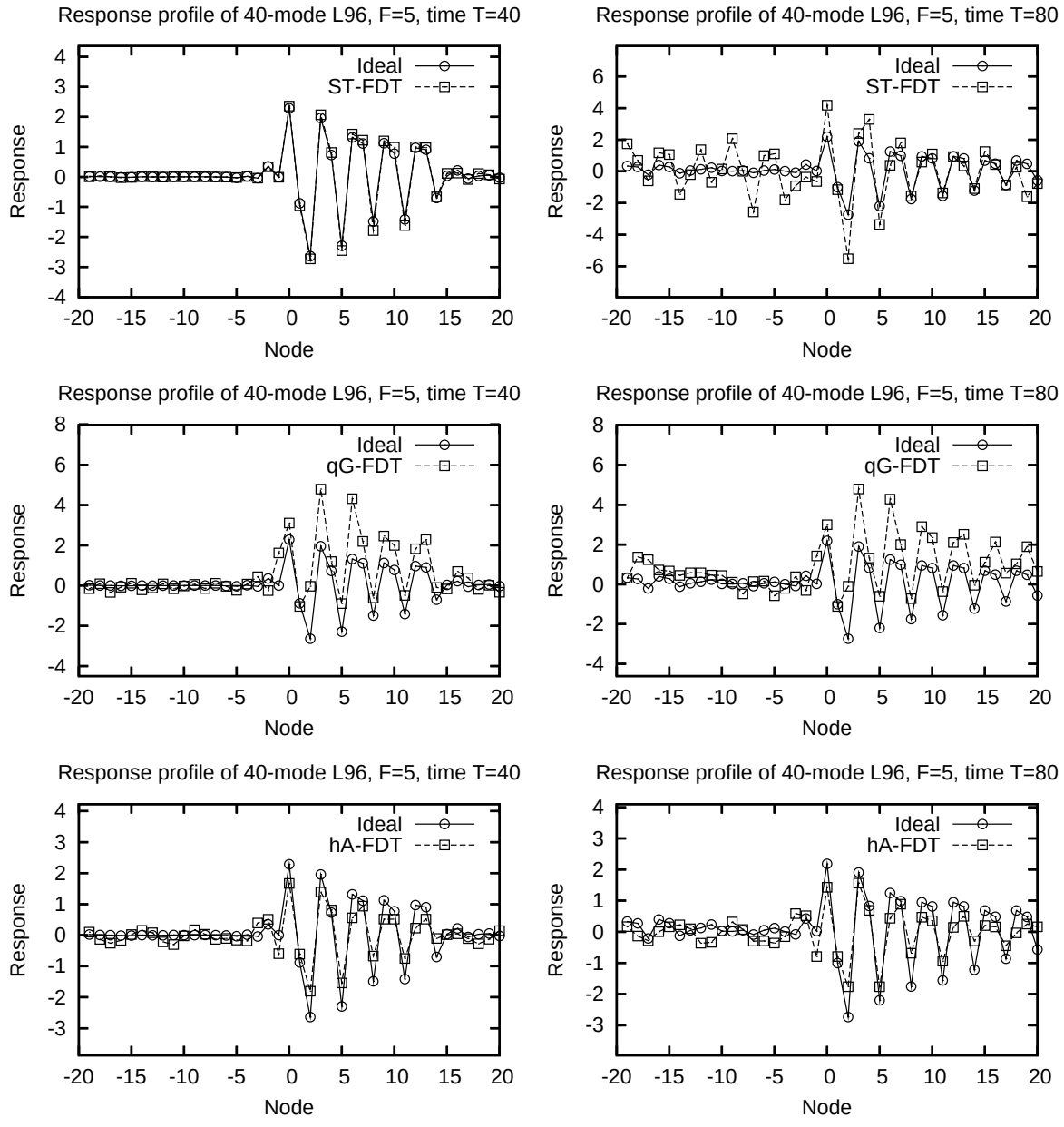

Figure 4. Profiles of the linear response operators for the regime $F = 5$, time $T = 40$ and $T = 80$, response function $A(\vec{x}) = \vec{x}$.

In Figures 6 and 7 we show the linear response operators in the physical space for the dynamical regimes with $F = 6$ and $F = 8$ at times $T = 2, 5, 10, 20, 40, 80$. Note that for short times $T \leq 10$ the qG-FDT linear response operator is better than the hA-FDT approximation. Theorem 2.3 in Chapter 2 of [17] guarantees that the error for linear response function in qG-FDT develops as $O(t^3)$, and what we observe here is presumably a manifestation of this fact. Nonetheless, the hA-FDT is better than the qG-FDT for longer times, $T = 40, 80$. These observations are confirmed below in Section 5 in Tables 3 and 5, where the L_2-errors and physical space correlations between the ideal operator and its FDT approximations are documented. The ST-FDT response

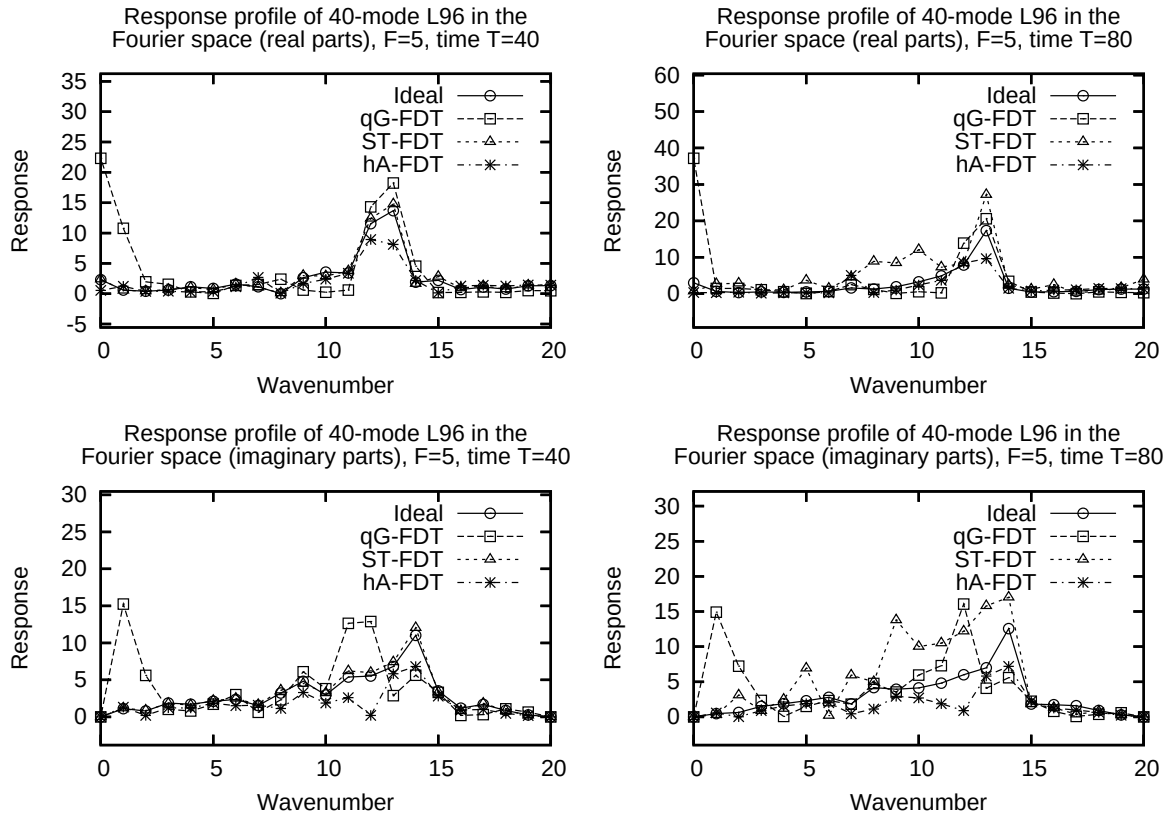

Figure 5. Profiles of the linear response operators in the Fourier space for the regime $F = 5$, time $T = 40$ and $T = 80$, response function $A(\vec{x}) = \vec{x}$.

operator is vastly superior to all other FDT approximations until the numerical blow-up, which is expected.

Although we do not show the plots with linear response operators for the turbulent self-similar regimes $F = 12, 16, 24$, the results for these dynamical regimes are summarized in Tables 4 and 6 below in Section 5, where the L_2-errors and physical space correlations are documented. For these dynamical regimes, at short times the situation is similar to that for $F = 5, 6, 8$, namely, the ST-FDT produces best results, and the performance of qG-FDT is better than that of hA-FDT. However, for long times the qG-FDT and hA-FDT approximations demonstrate comparable performance both in errors and correlations. Finally, we note that for $F = 5, 6, 8$ the hA-FDT response for the 40-mode L96 model is superior to the response in similar 5-mode models test in [2]. As listed in Table 1, the 40-mode models have a large-dimensional unstable manifold which allows for much more quasi-Gaussian averaging for the unstable dimensions in (2.28) compared to the 5-mode models in [2] with only two unstable directions.

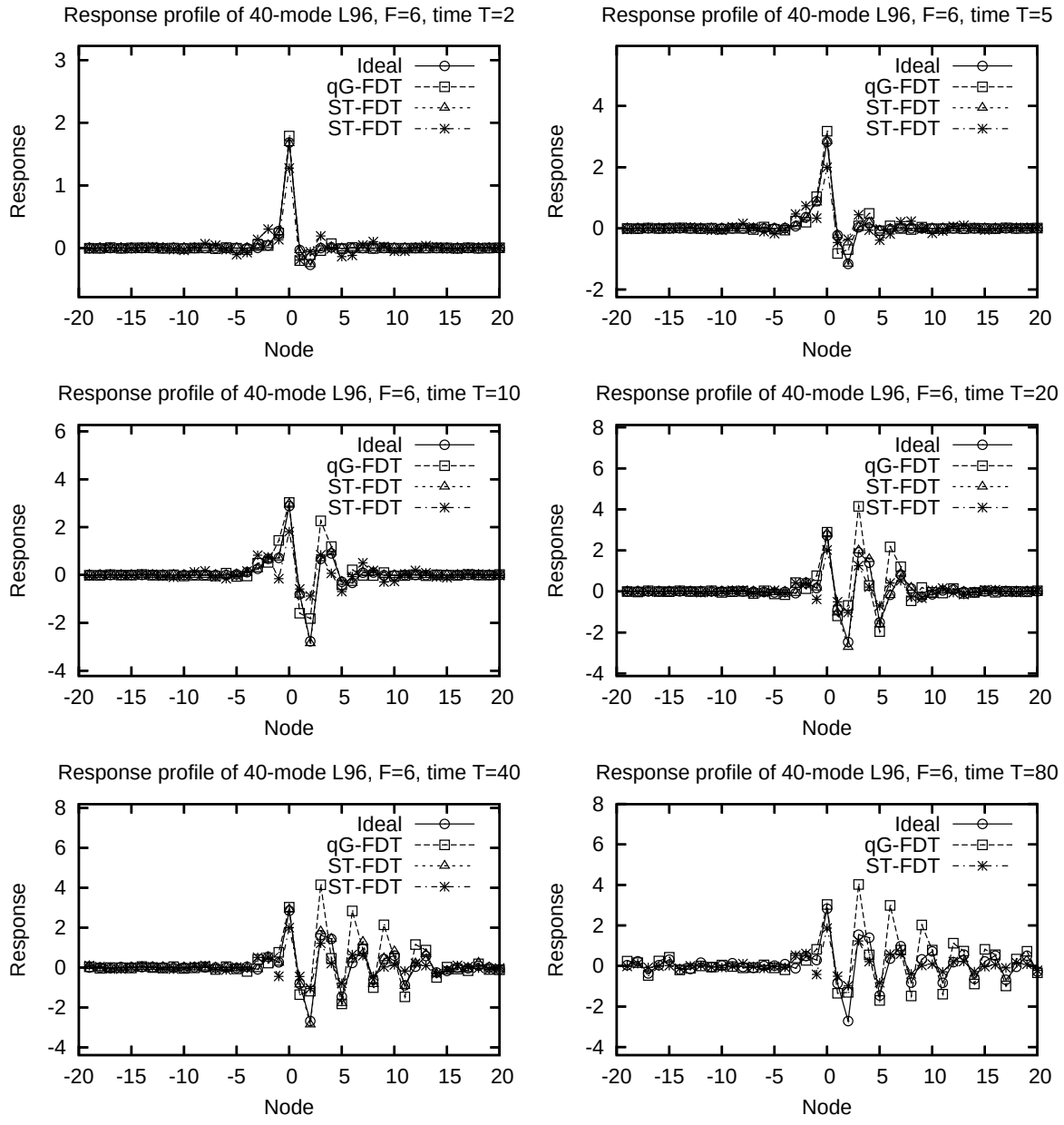

Figure 6. Profiles of the linear response operators for the regime $F = 6$, time $T = 2, 5, 10, 30, 40$ and 80, response function $A(\vec{x}) = \vec{x}$.

5. The blended response algorithms (BRA)

We observed in Section 4 that the ST-FDT linear response approximation and the qG-FDT or hA-FDT approximations have somewhat opposite advantages and drawbacks. Namely, while the ST-FDT is superior in all respects to both the qG-FDT and hA-FDT operators for short times, it eventually blows up for longer times due to inherent numerical instability. On the other hand, the qG-FDT and hA-FDT are free of numerical instabilities, but produce larger errors at short times. However, there is a simple way to avoid the blowup by blending the ST-FDT response with either qG-FDT or hA-FDT

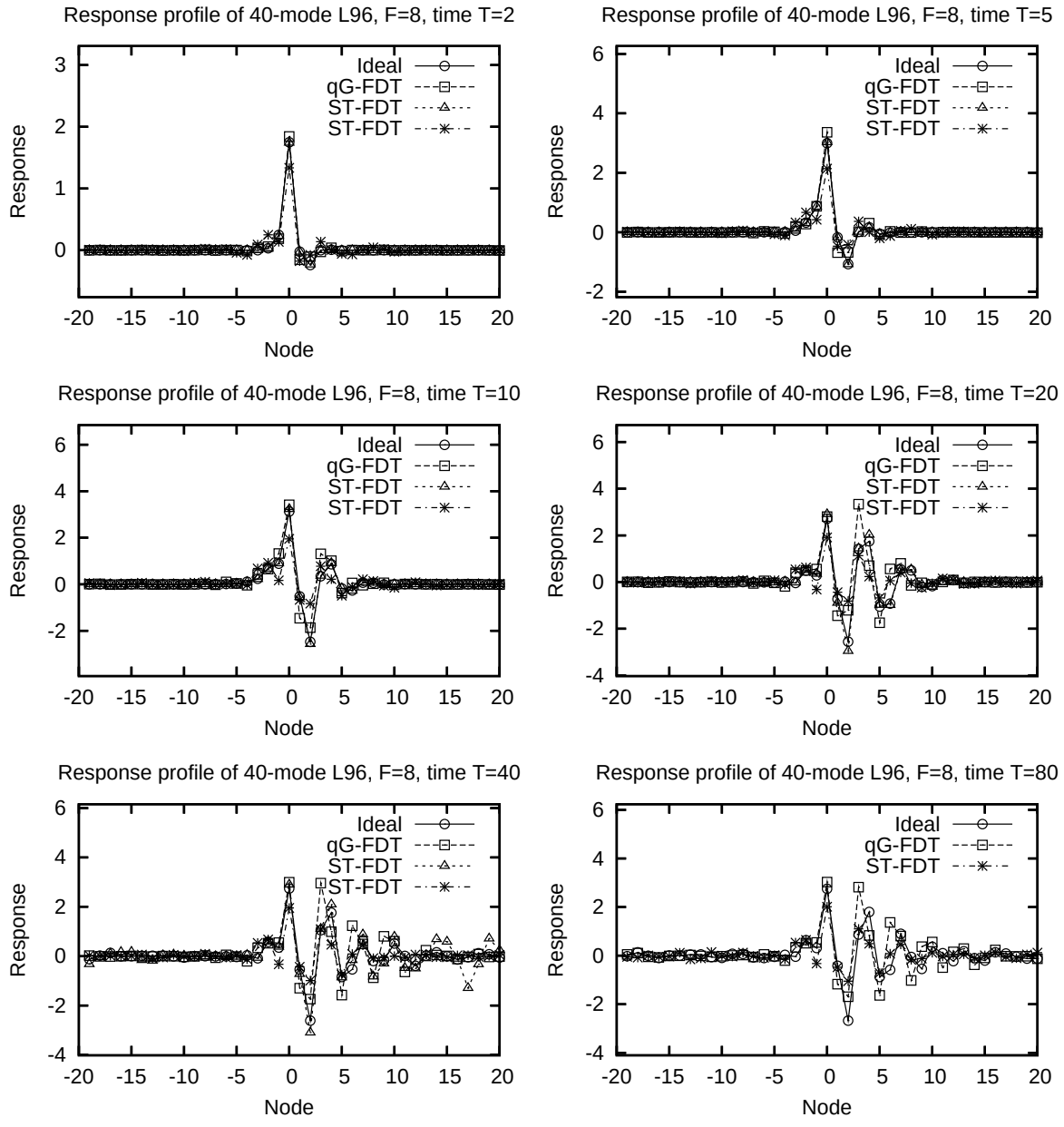

Figure 7. Profiles of the linear response operators for the regime $F = 8$, time $T = 2, 5, 10, 30, 40$ and 80, response function $A(\vec{x}) = \vec{x}$.

at later times before the numerical blow-up occurs, thus combining the best properties of both responses via the following formula:

$$\begin{aligned} R_{ST/qG} &= (1-\xi)R_{ST} + \xi R_{qG}, \\ R_{ST/hA} &= (1-\xi)R_{ST} + \xi R_{hA}, \end{aligned} \tag{5.1}$$

where $\xi = \xi(t)$ is a *blending function*, chosen so that it is zero for small values of t (thus the response at early times is computed through the highly accurate R_{ST} operator), and assumes the value of 1 shortly before the numerical instability manifests itself in R_{ST}. The simplest and most straightforward choice of the blending function is the Heaviside step-function

$$\xi(t) = H\left(t - T_{\text{cutoff}}\right), \tag{5.2}$$

where T_{cutoff} is the cutoff time chosen just before the numerical instability occurs in R_{ST}. The blended linear response operators $R_{ST/qG}$ and $R_{ST/hA}$ combine the advantages of the ST-FDT for shorter times, and qG-FDT and hA-FDT for longer times. For constant small external forcing $\delta f = const$ and the Heaviside blending step-function the blended response operators become

$$\mathcal{R}_{ST/qG}(T) = \int_0^{T_{\text{cutoff}}} R_{ST}(t)\mathrm{d}t + \int_{T_{\text{cutoff}}}^{T} R_{qG}(t)\mathrm{d}t, \tag{5.3a}$$

$$\mathcal{R}_{ST/hA}(T) = \int_0^{T_{\text{cutoff}}} R_{ST}(t)\mathrm{d}t + \int_{T_{\text{cutoff}}}^{T} R_{hA}(t)\mathrm{d}t. \tag{5.3b}$$

The Heaviside step-function (5.2) will be used as a blending function for (5.1) throughout the paper. Note, however, that the choice of the blending function $\xi(t)$ is not limited to the Heaviside function, and in fact, can be chosen systematically to minimize errors between observed test ideal response and linear response. A systematic adaptive algorithm for choosing optimal blending function $\xi(t)$ in a given particular setting will be developed by the authors in the near future.

With the choice of Heaviside step-function for blending, at this point the key question is to determine an appropriate cutoff time T_{cutoff} for a given dynamical regime. We know that the numerical instability occurs in ST-FDT due to certain subspaces of the tangent map growing exponentially fast, with the growth rate set forth by the largest Lyapunov exponent λ_1. Therefore, the blowup time T_{blowup} must be roughly proportional to the characteristic time of the largest Lyapunov exponent T_λ,

$$T_{\text{blowup}} \approx \alpha T_\lambda, \tag{5.4}$$

where the proportionality coefficient α depends on many factors, including details of numerical implementation of linear response correlation function, machine platform and type of floating point arithmetic used, but can be heuristically measured through direct numerical simulation. Here in Figure 8 we heuristically determine the proportionality coefficient between Lyapunov characteristic time and ST-FDT blowup time by superimposing these times on the graph for all tested dynamical regimes $F = 5, 6, 8, 12, 16, 24$ for the 40-mode Lorenz 96 model. As we can see in Figure 8, the

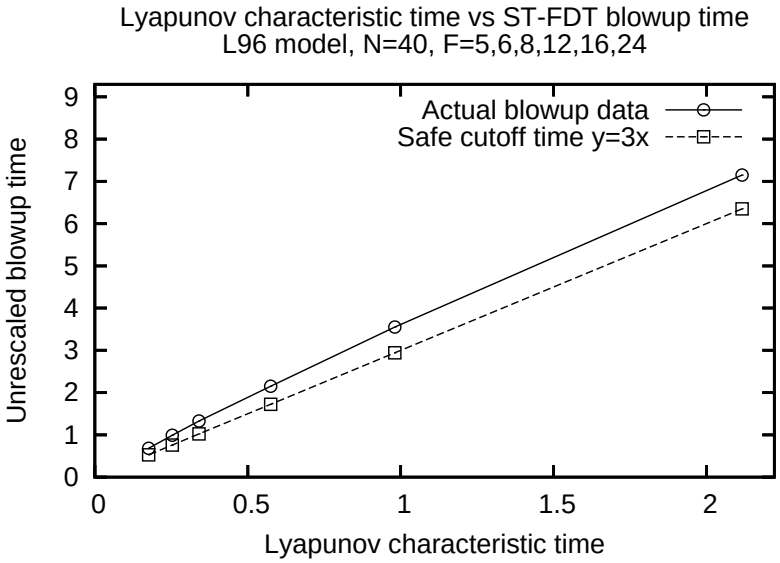

Computed ST-FDT cutoff times (energy-rescaled) 40-mode L96 model	
F	T_{cutoff}
$F = 5$	$T_{\text{cutoff}} = 66.58$
$F = 6$	$T_{\text{cutoff}} = 37.27$
$F = 8$	$T_{\text{cutoff}} = 28.06$
$F = 12$	$T_{\text{cutoff}} = 23.1$
$F = 16$	$T_{\text{cutoff}} = 21.47$
$F = 24$	$T_{\text{cutoff}} = 20.1$

Figure 8. The plot with blowup time vs Lyapunov characteristic time and heuristically computed cutoff times as $T_{\text{cutoff}} = 3T_\lambda$. The table shows computed rescaled cutoff times for each dynamical regime $F = 5, 6, 8, 12, 16, 24$.

scatter plot of blow-up time vs Lyapunov characteristic time for all dynamical regimes is nearly a straight line, as should be expected, with α slightly exceeding the value of 3. Thus, for the cutoff time T_{cutoff} computation we heuristically choose the formula

$$T_{\text{cutoff}} = 3T_\lambda, \tag{5.5}$$

such that each cutoff time is just below the blowup time (also shown in Figure 8). The table in Figure 8 shows heuristically computed rescaled times T_{cutoff} via the formula in (5.5).

In Figure 9 we show the snapshots of the blended ST/qG-FDT and ST/hA-FDT linear response approximations for the weakly chaotic dynamical regime $F = 6$, with cutoff time taken from the table in Figure 8, and compare them with the ideal response operator at the response time $T = 2, 5, 10, 20, 40, 80$. Observe that visually there is a remarkable improvement over the results in Figure 6, where the standalone qG-FDT, hA-

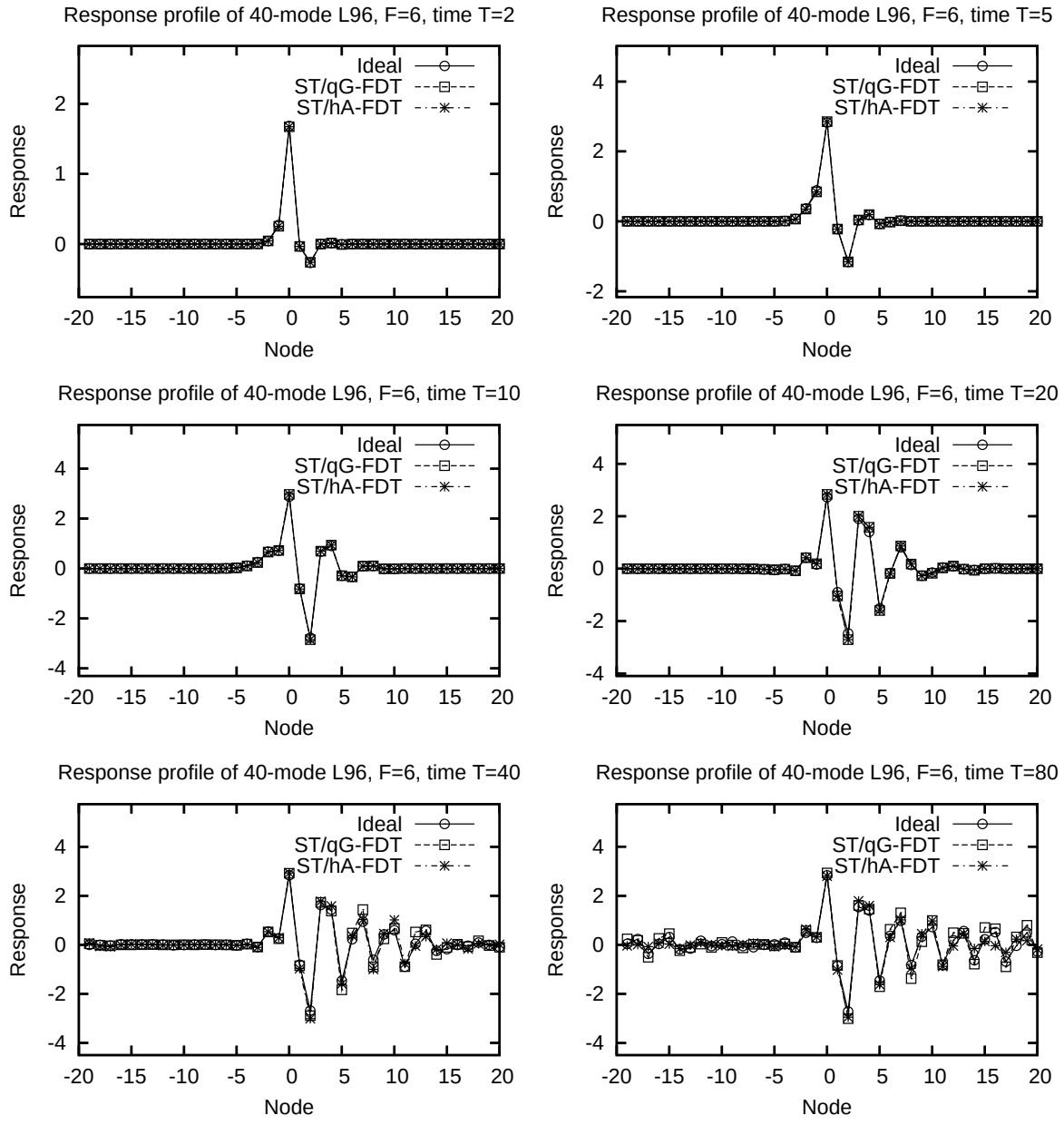

Figure 9. Profiles of the mixed linear response operators for the regime $F = 6$, time $T = 2, 5, 10, 30, 40$ and 80, response function $A(\vec{x}) = \vec{x}$.

FDT and ST-FDT approximations are displayed for the same dynamical regime. Also, in Figure 10 we demonstrate the snapshots of the blended ST/qG-FDT and ST/hA-FDT operators at time $T = 80$ for all studied dynamical regimes $F = 5, 6, 8, 12, 16, 24$. Taking into account that at $T = 80$ the response is roughly equivalent to the infinite time response (as established in Section 3), observe that there is again a remarkable visual improvement over the standalone qG-FDT and hA-FDT approximations, displayed in Section 4.

We summarize the results for all studied FDT approximations, all times and dynamical regimes in Tables 3, 4, 5 and 6, where Tables 3 and 4 contain the L_2-errors,

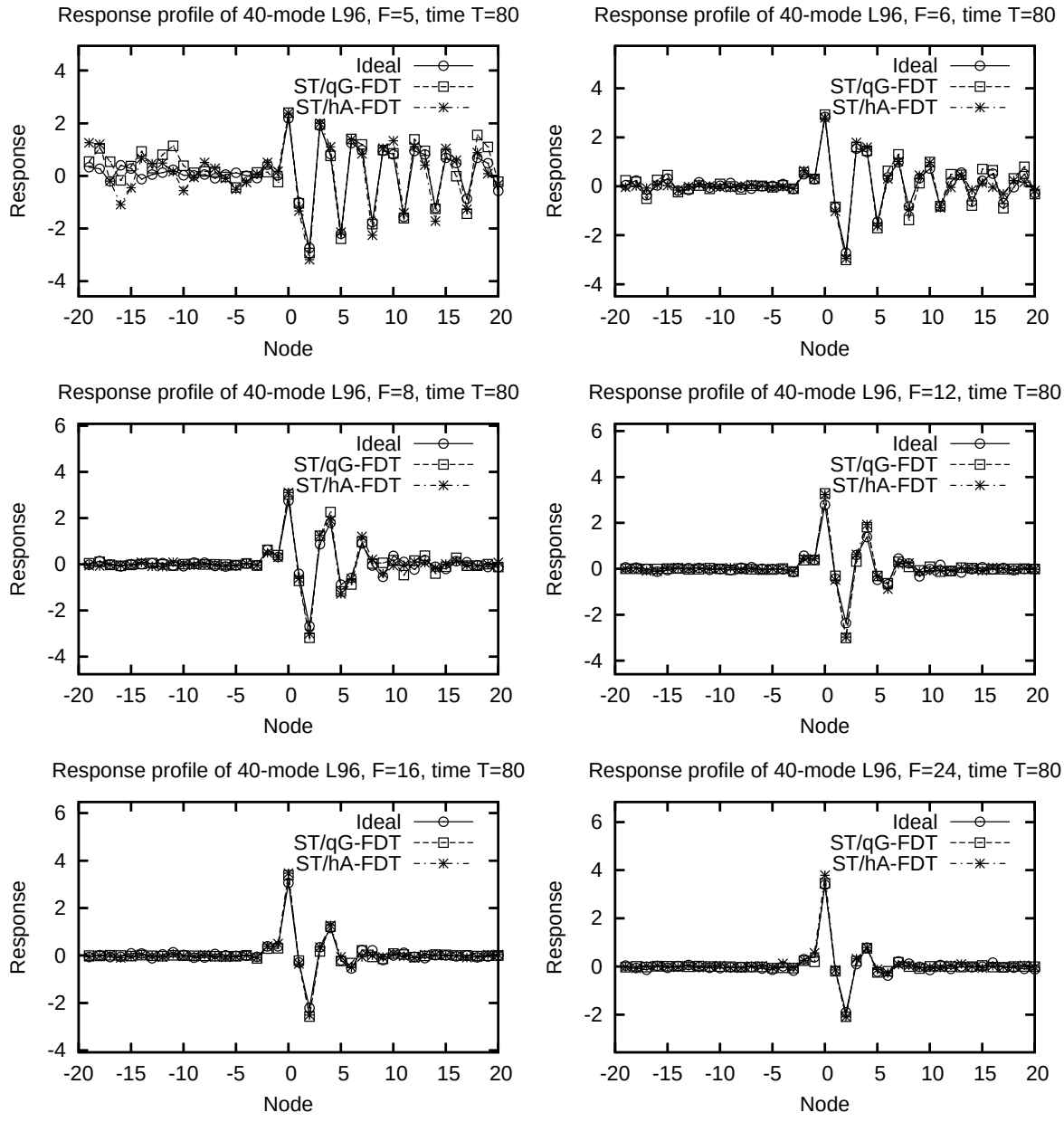

Figure 10. Profiles of the mixed linear response operators for the regimes $F = 5, 6, 8, 12, 16, 24$, time $T = 80$, response function $A(\vec{x}) = \vec{x}$.

and Tables 5 and 6 contain the physical space correlations between the ideal responses and various FDT approximations. Observe that the blended response approximations ST/qG-FDT and ST/hA-FDT are the same as the ST-FDT approximations before the cutoff time, but after the cutoff time the ST/qG-FDT and ST/hA-FDT blended response operators are vastly superior to any other FDT linear response approximations for all times and all dynamical regimes. Both ST/hA-FDT and ST/qG-FDT blended approximations provide comparable error reduction for longer times (roughly by a factor of 2-3 compared to standalone qG-FDT and hA-FDT) with relative L_2-errors not exceeding 30% for dynamical regimes with $F \geq 6$, and diminishing to 14-18%

for turbulent self-similar regimes $F = 16, 24$. A remarkable improvement can also be observed for physical space correlations: for the dynamical regimes with $F \geq 6$ the physical space correlations exceed 0.97 for all times, reaching values of 0.99 at $T = 80$ for turbulent regimes $F = 16, 24$.

6. The blended response algorithm: Nonlinear response functions

All linear response approximations, developed in Section 2, are designed to work with an arbitrary (although differentiable) response function. So far in Sections 4 and 5 we demonstrated the ability of the new linear response approximations to predict the response of a simple linear function $A(\vec{x}) = \vec{x}$, which corresponds to the response of the long-term mean state of the dynamical system to small changes in external forcing.

Response L_2-error values of 40-mode L96, F=5					
Time	ST-FDT	qG-FDT	hA-FDT	ST/qG-FDT	ST/hA-FDT
2	$1.832 \cdot 10^{-2}$	0.2058	0.6041	$1.832 \cdot 10^{-2}$	$1.832 \cdot 10^{-2}$
5	$2.013 \cdot 10^{-2}$	0.4901	0.7851	$2.013 \cdot 10^{-2}$	$2.013 \cdot 10^{-2}$
10	$3.055 \cdot 10^{-2}$	0.8194	0.7805	$3.055 \cdot 10^{-2}$	$3.055 \cdot 10^{-2}$
20	0.05841	0.9949	0.3447	0.05841	0.05841
40	0.09481	1.083	0.4336	0.09481	0.09481
80	1.157	1.252	0.522	0.4274	0.4752

Response L_2-error values of 40-mode L96, F=6					
Time	ST-FDT	qG-FDT	hA-FDT	ST/qG-FDT	ST/hA-FDT
2	$1.399 \cdot 10^{-2}$	0.1587	0.391	$1.399 \cdot 10^{-2}$	$1.399 \cdot 10^{-2}$
5	$1.651 \cdot 10^{-2}$	0.2937	0.5012	$1.651 \cdot 10^{-2}$	$1.651 \cdot 10^{-2}$
10	$3.078 \cdot 10^{-2}$	0.5198	0.6178	$3.078 \cdot 10^{-2}$	$3.078 \cdot 10^{-2}$
20	0.07751	0.8485	0.5304	0.07751	0.07751
40	0.1386	0.9245	0.5548	0.1852	0.1679
80	$--$	0.8872	0.5784	0.2399	0.2396

Response L_2-error values of 40-mode L96, F=8					
Time	ST-FDT	qG-FDT	hA-FDT	ST/qG-FDT	ST/hA-FDT
2	$1.003 \cdot 10^{-2}$	0.1285	0.3216	$1.003 \cdot 10^{-2}$	$1.003 \cdot 10^{-2}$
5	$1.432 \cdot 10^{-2}$	0.2334	0.4139	$1.432 \cdot 10^{-2}$	$1.432 \cdot 10^{-2}$
10	0.03735	0.3827	0.5557	0.03735	0.03735
20	0.122	0.6877	0.6104	0.122	0.122
40	0.4549	0.7383	0.5726	0.3525	0.3047
80	$--$	0.7826	0.5686	0.3072	0.2513

Table 3. The L_2-errors between the linear response approximations and the ideal response, dynamical regimes $F = 5, 6, 8$, response function $A(\vec{x}) = \vec{x}$.

Response L_2-error values of 40-mode L96, F=12					
Time	ST-FDT	qG-FDT	hA-FDT	ST/qG-FDT	ST/hA-FDT
2	$1.432 \cdot 10^{-2}$	0.1041	0.2785	$1.432 \cdot 10^{-2}$	$1.432 \cdot 10^{-2}$
5	$1.401 \cdot 10^{-2}$	0.1825	0.3405	$1.401 \cdot 10^{-2}$	$1.401 \cdot 10^{-2}$
10	$3.048 \cdot 10^{-2}$	0.2819	0.4538	$3.048 \cdot 10^{-2}$	$3.048 \cdot 10^{-2}$
20	0.0977	0.5245	0.572	0.0977	0.0977
40	0.5547	0.5328	0.5531	0.2531	0.2
80	$--$	0.5181	0.5188	0.2766	0.2684

Response L_2-error values of 40-mode L96, F=16					
Time	ST-FDT	qG-FDT	hA-FDT	ST/qG-FDT	ST/hA-FDT
2	$1.224 \cdot 10^{-2}$	0.09162	0.2502	$1.224 \cdot 10^{-2}$	$1.224 \cdot 10^{-2}$
5	$1.274 \cdot 10^{-2}$	0.1614	0.3017	$1.274 \cdot 10^{-2}$	$1.274 \cdot 10^{-2}$
10	$3.065 \cdot 10^{-2}$	0.241	0.3959	$3.065 \cdot 10^{-2}$	$3.065 \cdot 10^{-2}$
20	0.1062	0.4208	0.4858	0.1062	0.1062
40	1.827	0.4927	0.5459	0.1343	0.1519
80	$--$	0.4486	0.5175	0.1805	0.1899

Response L_2-error values of 40-mode L96, F=24					
Time	ST-FDT	qG-FDT	hA-FDT	ST/qG-FDT	ST/hA-FDT
2	$1.019 \cdot 10^{-2}$	0.07962	0.2144	$1.019 \cdot 10^{-2}$	$1.019 \cdot 10^{-2}$
5	$1.199 \cdot 10^{-2}$	0.1424	0.2572	$1.199 \cdot 10^{-2}$	$1.199 \cdot 10^{-2}$
10	$2.787 \cdot 10^{-2}$	0.2028	0.338	$2.787 \cdot 10^{-2}$	$2.787 \cdot 10^{-2}$
20	0.1051	0.3085	0.3992	0.09308	0.09934
40	1.767	0.3978	0.4699	0.1494	0.2049
80	$--$	0.3708	0.4449	0.14	0.1796

Table 4. The L_2-errors between the linear response approximations and the ideal response, dynamical regimes $F = 12, 16, 24$, response function $A(\vec{x}) = \vec{x}$.

Response *Corr* values of 40-mode L96, F=5					
Time	ST-FDT	qG-FDT	hA-FDT	ST/qG-FDT	ST/hA-FDT
2	0.9999	0.9812	0.8068	0.9999	0.9999
5	0.9998	0.9087	0.6777	0.9998	0.9998
10	0.9999	0.7746	0.6621	0.9999	0.9999
20	0.9996	0.7439	0.9655	0.9996	0.9996
40	0.9983	0.7231	0.937	0.9983	0.9983
80	0.8012	0.6467	0.8771	0.9346	0.9217

Response *Corr* values of 40-mode L96, F=6					
Time	ST-FDT	qG-FDT	hA-FDT	ST/qG-FDT	ST/hA-FDT
2	0.9999	0.9895	0.9294	0.9999	0.9999
5	0.9999	0.966	0.8745	0.9999	0.9999
10	0.9999	0.888	0.8068	0.9999	0.9999
20	0.9994	0.753	0.8932	0.9994	0.9994
40	0.995	0.7633	0.8767	0.9884	0.9911
80	$--$	0.787	0.8708	0.9827	0.9736

Response *Corr* values of 40-mode L96, F=8					
Time	ST-FDT	qG-FDT	hA-FDT	ST/qG-FDT	ST/hA-FDT
2	1	0.9931	0.964	1	1
5	0.9999	0.979	0.9319	0.9999	0.9999
10	0.9999	0.9387	0.8636	0.9999	0.9999
20	0.9976	0.7935	0.8328	0.9976	0.9976
40	0.9337	0.7895	0.8536	0.9696	0.9673
80	$--$	0.7498	0.8535	0.9741	0.9804

Table 5. The physical space correlations between the linear response approximations and the ideal response, dynamical regimes $F = 5, 6, 8$, response function $A(\vec{x}) = \vec{x}$.

Response *Corr* values of 40-mode L96, F=12					
Time	ST-FDT	qG-FDT	hA-FDT	ST/qG-FDT	ST/hA-FDT
2	1	0.9951	0.9815	1	1
5	0.9999	0.9867	0.9658	0.9999	0.9999
10	0.9999	0.968	0.9248	0.9999	0.9999
20	0.9992	0.8753	0.8482	0.9992	0.9992
40	0.8998	0.8635	0.8596	0.9791	0.9907
80	−−	0.8808	0.8766	0.9812	0.9864

Response *Corr* values of 40-mode L96, F=16					
Time	ST-FDT	qG-FDT	hA-FDT	ST/qG-FDT	ST/hA-FDT
2	1	0.9962	0.988	1	1
5	0.9999	0.9898	0.976	0.9999	0.9999
10	0.9999	0.9776	0.9467	0.9999	0.9999
20	0.9982	0.9236	0.8993	0.9982	0.9982
40	0.4928	0.8799	0.8624	0.9917	0.9915
80	−−	0.9091	0.8748	0.9892	0.9902

Response *Corr* values of 40-mode L96, F=24					
Time	ST-FDT	qG-FDT	hA-FDT	ST/qG-FDT	ST/hA-FDT
2	1	0.9971	0.9933	1	1
5	0.9999	0.9921	0.9849	0.9999	0.9999
10	0.9999	0.9853	0.9657	0.9999	0.9999
20	0.9986	0.9635	0.94	0.9989	0.9988
40	0.5567	0.9255	0.8997	0.9889	0.9842
80	−−	0.9366	0.9121	0.9906	0.9901

Table 6. The physical space correlations between the linear response approximations and the ideal response, dynamical regimes $F = 12, 16, 24$, response function $A(\vec{x}) = \vec{x}$.

However, in geophysical applications such as climate change prediction, the response of the local variance, which is a quadratic function of phase space coordinates, is also important [11]. In this section we present the study of the linear response of a simple vector-valued quadratic function $A_i(\vec{x}) = x_i^2$ to small external forcing, where $\vec{x}$ is a vector of phase space coordinates.

Recall from Section 2 that the hA-FDT approximation is vastly more expensive to compute than the qG-FDT approximation, and even more expensive than the ST-FDT approximation. However, previously in Section 5 we found that the blended ST/qG and ST/hA FDT approximations yield roughly comparable results for a simple linear response function. With that in mind, here we abandon the ST/hA-FDT approximation as excessively computationally costly, and instead study the ST/qG-FDT blended approximation, which is of comparable precision yet cheap to compute.

In Figure 11 we show the snapshots of the blended ST/qG-FDT linear response approximations to the quadratic response function for the weakly chaotic dynamical regime $F = 6$, with cutoff time taken from the table in Figure 8, and compare them with the ideal response operator at the response time $T = 2, 5, 10, 20, 40, 80$. Observe that visually there is a remarkable precision achieved with the blended ST/qG-FDT response operator. Also, in Figure 12 we demonstrate the snapshots of the blended ST/qG-FDT operator at time $T = 80$ for all studied dynamical regimes $F = 5, 6, 8, 12, 16, 24$. Taking into account that at $T = 80$ the response is roughly equivalent to the infinite time response (as established in Section 3), observe that there is again a remarkable precision achieved for long-time linear response of the quadratic function in a variety of different dynamical regimes.

We summarize the results for all studied FDT approximations, all times and dynamical regimes in Tables 7 and 8, which contain the L_2-errors and physical space correlations between the ideal responses and various FDT approximations. Observe that the blended response approximation ST/qG-FDT is the same as the ST-FDT approximations before the cutoff time, but after the cutoff time the ST/qG-FDT blended response operator is vastly superior to any other FDT linear response approximation for all times and all dynamical regimes. The ST/hA-FDT blended approximation provides substantial error reduction for longer times (roughly by a factor of 2-3 compared to the standalone qG-FDT) with relative L_2-errors not exceeding 28% for dynamical regimes with $F \geq 6$, and diminishing to 14-18% for turbulent self-similar regimes $F = 16, 24$. A remarkable improvement can also be observed for physical space correlations: for the dynamical regimes with $F \geq 6$ the physical space correlations exceed 0.97 for all times, reaching values of 0.99 at $T = 80$ for turbulent regimes $F = 16, 24$.

7. Summary

In a recent paper [2] we developed two new approaches, the short-time FDT (ST-FDT) and the hybrid Axiom A FDT (hA-FDT), for predicting linear response of a nonlinear chaotic forced-dissipative system to small external forcing. In the current work we

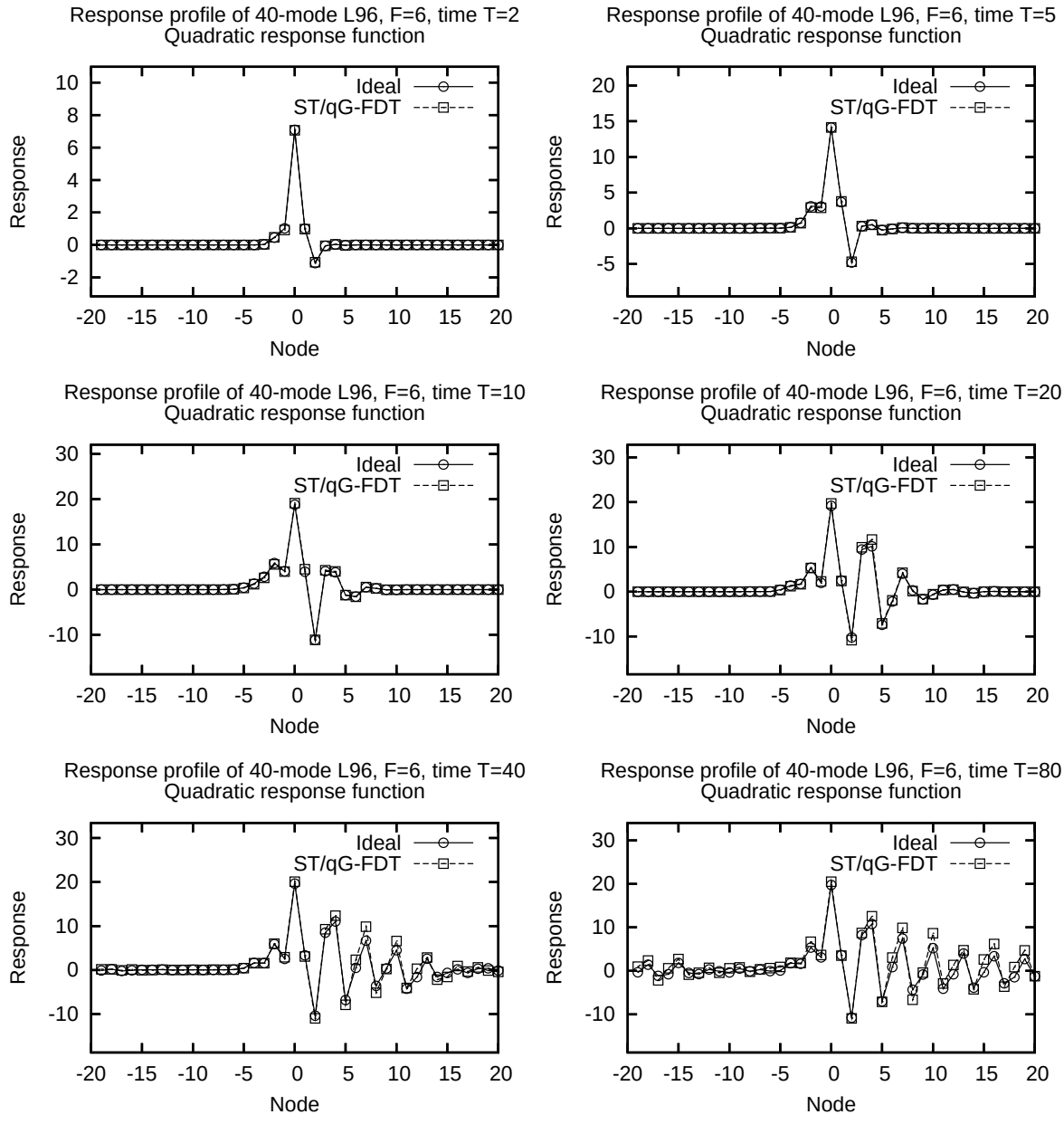

Figure 11. Profiles of the mixed linear response operators for the regime $F = 6$, time $T = 2, 5, 10, 30, 40$ and 80, quadratic response function $A_i(\vec{x}) = x_i^2$.

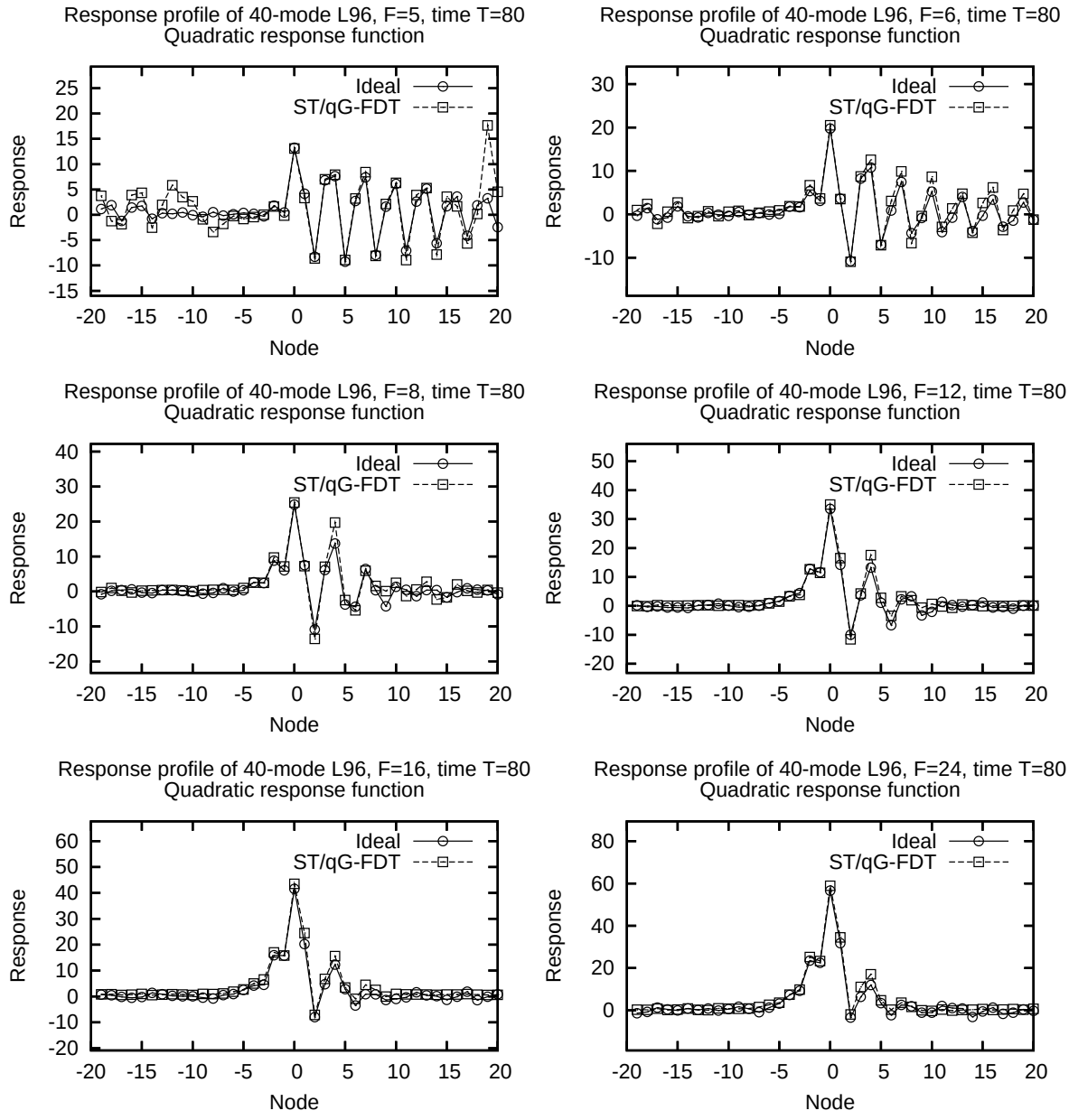

Figure 12. Profiles of the mixed linear response operators for the regimes $F = 5, 6, 8, 12, 16, 24$, time $T = 80$, quadratic response function $A_i(\vec{x}) = \vec{x}_i^2$.

Response L_2-error of 40-mode L96 F=5, quadratic response function			
Time	ST	qG	ST/qG
2	$2.283 \cdot 10^{-2}$	0.5336	$2.283 \cdot 10^{-2}$
5	$1.899 \cdot 10^{-2}$	0.5649	$1.899 \cdot 10^{-2}$
10	$2.723 \cdot 10^{-2}$	0.6482	$2.723 \cdot 10^{-2}$
20	$5.645 \cdot 10^{-2}$	0.8883	$5.645 \cdot 10^{-2}$
40	0.1021	1.068	0.1021
80	2.064	1.123	0.6943

Response *Corr* of 40-mode L96 F=5, quadratic response function			
Time	ST	qG	ST/qG
2	0.9998	0.8882	0.9998
5	0.9998	0.8735	0.9998
10	0.9997	0.8854	0.9997
20	0.9991	0.8571	0.9991
40	0.9977	0.7926	0.9977
80	0.4923	0.7485	0.8465

Response L_2-error of 40-mode L96 F=6, quadratic response function			
Time	ST	qG	ST/qG
2	$1.597 \cdot 10^{-2}$	0.3014	$1.597 \cdot 10^{-2}$
5	$1.94 \cdot 10^{-2}$	0.2984	$1.94 \cdot 10^{-2}$
10	$3.442 \cdot 10^{-2}$	0.3886	$3.442 \cdot 10^{-2}$
20	$6.776 \cdot 10^{-2}$	0.6866	$6.776 \cdot 10^{-2}$
40	0.1896	0.8312	0.1841
80	$--$	0.8267	0.2777

Response *Corr* of 40-mode L96 F=6, quadratic response function			
Time	ST	qG	ST/qG
2	0.9999	0.9595	0.9999
5	0.9998	0.9586	0.9998
10	0.9995	0.9424	0.9995
20	0.9987	0.8595	0.9987
40	0.9891	0.8422	0.9891
80	$--$	0.8459	0.9747

Response L_2-error of 40-mode L96 F=8, quadratic response function			
Time	ST	qG	ST/qG
2	$1.142 \cdot 10^{-2}$	0.2481	$1.142 \cdot 10^{-2}$
5	$1.514 \cdot 10^{-2}$	0.2278	$1.514 \cdot 10^{-2}$
10	$3.244 \cdot 10^{-2}$	0.2761	$3.244 \cdot 10^{-2}$
20	$9.782 \cdot 10^{-2}$	0.5234	$9.782 \cdot 10^{-2}$
40	0.3684	0.5757	0.2819
80	$--$	0.5914	0.2869

Response *Corr* of 40-mode L96 F=8, quadratic response function			
Time	ST	qG	ST/qG
2	0.9999	0.9725	0.9999
5	0.9999	0.9759	0.9999
10	0.9996	0.9675	0.9996
20	0.9977	0.8872	0.9977
40	0.9467	0.8733	0.9735
80	$--$	0.8633	0.9704

Table 7. The L_2-errors between the linear response approximations and the ideal response, dynamical regimes $F = 5, 6, 8$, quadratic response function $A_i(\vec{x}) = \vec{x}_i^2$.

Response L_2-error of 40-mode L96 F=12, quadratic response function			
Time	ST	qG	ST/qG
2	$1.55 \cdot 10^{-2}$	0.2175	$1.55 \cdot 10^{-2}$
5	$1.512 \cdot 10^{-2}$	0.1976	$1.512 \cdot 10^{-2}$
10	$2.998 \cdot 10^{-2}$	0.2058	$2.998 \cdot 10^{-2}$
20	$9.725 \cdot 10^{-2}$	0.3354	$9.725 \cdot 10^{-2}$
40	1.084	0.3711	0.1674
80	$--$	0.3862	0.186

Response *Corr* of 40-mode L96 F=12, quadratic response function			
Time	ST	qG	ST/qG
2	0.9999	0.9807	0.9999
5	0.9999	0.9833	0.9999
10	0.9996	0.9818	0.9996
20	0.997	0.9493	0.997
40	0.7306	0.9372	0.9902
80	$--$	0.93	0.9859

Response L_2-error of 40-mode L96 F=16, quadratic response function			
Time	ST	qG	ST/qG
2	$1.686 \cdot 10^{-2}$	0.2089	$1.686 \cdot 10^{-2}$
5	$1.691 \cdot 10^{-2}$	0.1923	$1.691 \cdot 10^{-2}$
10	$2.705 \cdot 10^{-2}$	0.1915	$2.705 \cdot 10^{-2}$
20	$6.755 \cdot 10^{-2}$	0.2487	$6.755 \cdot 10^{-2}$
40	1.156	0.2809	0.1471
80	$--$	0.2899	0.1818

Response *Corr* of 40-mode L96 F=16, quadratic response function			
Time	ST	qG	ST/qG
2	0.9999	0.9833	0.9999
5	0.9999	0.9851	0.9999
10	0.9997	0.9849	0.9997
20	0.9983	0.9713	0.9983
40	0.6379	0.962	0.9901
80	$--$	0.9642	0.9883

Response L_2-error of 40-mode L96 F=24, quadratic response function			
Time	ST	qG	ST/qG
2	$9.594 \cdot 10^{-3}$	0.2176	$9.594 \cdot 10^{-3}$
5	$9.824 \cdot 10^{-3}$	0.2045	$9.824 \cdot 10^{-3}$
10	$2.125 \cdot 10^{-2}$	0.1969	$2.125 \cdot 10^{-2}$
20	$7.839 \cdot 10^{-2}$	0.1867	$7.03 \cdot 10^{-2}$
40	1.979	0.2194	0.1427
80	$--$	0.214	0.1458

Response *Corr* of 40-mode L96 F=24, quadratic response function			
Time	ST	qG	ST/qG
2	1	0.9842	1
5	1	0.9847	1
10	0.9998	0.9847	0.9998
20	0.9976	0.9838	0.998
40	0.4941	0.9773	0.9911
80	$--$	0.9799	0.9922

Table 8. The L_2-errors between the linear response approximations and the ideal response, dynamical regimes $F = 12, 16, 24$, quadratic response function $A_i(\vec{x}) = \vec{x}_i^2$.

design and test a new accurate and numerically stable strategy for predicting linear response of a chaotic nonlinear dynamical system with forcing and dissipation to small external perturbation through long-term observations of behavior of the unperturbed model. The approach is based on blending the general linear response formula at short time, which is suitable for predicting the linear response for an arbitrary dynamical system, with different approximations of the fluctuation-dissipation theorem at longer times. The cutoff time for blended linear response operators is computed via a simple universal formula, which is based on the characteristic time of the largest Lyapunov exponent.

In Sections 5 and 6, the blended methods are tested for a simple linear and quadratic response functions, compared with the classical quasi-Gaussian FDT (qG-FDT) and standalone short-time FDT (ST-FDT) and hybrid Axiom A FDT (hA-FDT) formulas, described in Section 2 and verified in Section 4 against the ideal directly measured response for the 40-mode Lorenz 96 system, described in Section 3, in a variety of weakly, moderately and strongly chaotic dynamical regimes. It is found that the blended ST/qG-FDT and ST/hA-FDT algorithms are vastly superior to the standalone ST-FDT, qG-FDT and hA-FDT algorithms even for long-term and infinite time linear response. Also, the blended ST/qG-FDT algorithm is found to be moderately computationally expensive, compared to the standalone qG-FDT. Furthermore, the accuracy of the ST/qG-FDT blended algorithm did not deteriorate for the response of linear and quadratic functions through all regimes of chaotic behavior. All of these facts suggest the implementation of the ST/qG-FDT blended response algorithm in more sophisticated nonlinear models.

Future research in this direction will be centered at developing systematic adaptive algorithms for choosing optimal blending function for linear response in a variety of practical settings, as well as testing the blended response algorithms for more sophisticated models with large-scale features of the real atmosphere and climate, like the T21 truncation of the barotropic quasigeostrophic equations on the sphere with realistic orography and forcing, or the 1.5-layer quasigeostrophic double-gyre model, which describes the wind-stress driven large-scale oceanic flows.

Acknowledgments

Rafail Abramov is supported by the NSF grant DMS-0608984 and the ONR grant N00014-06-1-0286. Andrew Majda is partially supported by the NSF grant DMS-0456713 and the ONR grant N00014-05-1-0164.

[1] R. Abramov and A. Majda. Quantifying uncertainty for non-Gaussian ensembles in complex systems. *SIAM J. Sci. Comp.*, 26(2):411–447, 2003.

[2] R. Abramov and A. Majda. New approximations and tests of linear fluctuation-response for chaotic nonlinear forced-dissipative dynamical systems. *J. Nonlin. Sci.*, 2007. submitted.

[3] T. Bell. Climate sensitivity from fluctuation dissipation: Some simple model tests. *J. Atmos. Sci.*, 37(8):1700–1708, 1980.

[4] G. Carnevale, M. Falcioni, S. Isola, R. Purini, and A. Vulpiani. Fluctuation-response in systems with chaotic behavior. *Phys. Fluids A*, 3(9):2247–2254, 1991.

[5] B. Cohen and G. Craig. The response time of a convective cloud ensemble to a change in forcing. *Quart. J. Roy. Met. Soc.*, 130(598):933–944, 2004.

[6] J. Eckmann and D. Ruelle. Ergodic theory of chaos and strange attractors. *Rev. Mod. Phys.*, 57(3):617–656, 1985.

[7] D. Evans and G. Morriss. *Statistical Mechanics of Nonequilibrium Liquids*. Academic Press, New York, 1990.

[8] A. Gritsoun. Fluctuation-dissipation theorem on attractors of atmospheric models. *Russ. J. Numer. Math. Modeling*, 16(2):115–133, 2001.

[9] A. Gritsoun and G. Branstator. Climate response using a three-dimensional operator based on the fluctuation-dissipation theorem. *J. Atmos. Sci.*, 2007. Accepted for publication.

[10] A. Gritsoun, G. Branstator, and V. Dymnikov. Construction of the linear response operator of an atmospheric general circulation model to small external forcing. *Num. Anal. Math. Modeling*, 17:399–416, 2002.

[11] A. Gritsoun, G. Branstator, and A. Majda. Climate response of linear and quadratic functionals using the fluctuation dissipation theorem. Submitted to *J. Atmos. Sci.*, 2007.

[12] A. Gritsoun and V. Dymnikov. Barotropic atmosphere response to small external actions. theory and numerical experiments. *Atmos. Ocean Phys.*, 35(5):511–525, 1999.

[13] R. Kubo, M. Toda, and N. Hashitsume. *Statistical Physics II: Nonequilibrium Statistical Mechanics*. Springer-Verlag, New York, 1985.

[14] C. Leith. Climate response and fluctuation-dissipation. *J. Atmos. Sci.*, 32:2022–2025, 1975.

[15] E. Lorenz. Predictability: A problem partly solved. In *Proceedings of the Seminar on Predictability*, Shinfield Park, Reading, England, 1996. ECMWF.

[16] E. Lorenz and K. Emanuel. Optimal sites for supplementary weather observations. *J. Atmos. Sci.*, 55:399–414, 1998.

[17] A. Majda, R. Abramov, and M. Grote. *Information Theory and Stochastics for Multiscale Nonlinear Systems*, volume 25 of *CRM Monograph Series of Centre de Recherches Mathématiques, Université de Montréal*. American Mathematical Society, 2005. ISBN 0-8218-3843-1.

[18] S. Orszag and J. McLaughlin. Evidence that random behavior is generic for nonlinear differential equations. *Physica D*, 1:68–79, 1980.

[19] F. Risken. *The Fokker-Planck Equation*. Springer-Verlag, New York, second edition, 1988.

[20] D. Ruelle. Differentiation of SRB states. *Comm. Math. Phys.*, 187:227–241, 1997.

[21] D. Ruelle. General linear response formula in statistical mechanics, and the fluctuation-dissipation theorem far from equilibrium. *Phys. Lett. A*, 245:220–224, 1998.

[22] L.-S. Young. What are SRB measures, and which dynamical systems have them? *J. Stat. Phys.*, 108(5-6):733–754, 2002.